Journal of Clinical Neurophysiology
18(3):223–245, Lippincott Williams & Wilkins, Inc., Philadelphia
© 2001 American Clinical Neurophysiology Society

Epileptic Event Forewarning From Scalp EEG

*Vladimir A. Protopopescu, *Lee M. Hively, and †Paul C. Gailey

** Oak Ridge National Laboratory, Oak Ridge, Tennessee; and the †Department of Physics and Astronomy, Ohio University, Athens, Ohio, U.S.A.*

The authors present a model-independent approach to quantify changes in the dynamics underlying nonlinear time-serial data. From time-windowed datasets, the authors construct discrete distribution functions on the phase space. Condition change between base case and test case distribution functions is assessed by dissimilarity measures via L_1 distance and χ^2 statistic. The discriminating power of these measures is first tested on noiseless data from the Lorenz and Bondarenko models, and is then applied to detecting dynamic change in multichannel clinical scalp EEG data. The authors compare the dissimilarity measures with the traditional nonlinear measures used in the analysis of chaotic systems. They also assess the potential usefulness of the new measures for robust, accurate, and timely forewarning of epileptic events. **Key Words:** Nonlinear measures—Event forewarning—Scalp EEG—Artifact filter.

Physiologic systems in either normal or pathologic conditions display a very rich variety of dynamic behaviors. These behaviors manifest themselves in signals that can be interpreted at various levels; namely, clinical, physiologic, chemical, physical, and so forth. During the last two decades, since the advent of chaotic dynamics on the scientific stage, we have witnessed a strong, reenergized interest in casting and interpreting physiologic data within a dynamic systems framework. Such a dynamic approach is motivated by several features that are shared by physiologic and complex systems; namely, multiple time scales, quasiperiodicity, chaos, and self-organization. Typically, complex systems (1) comprise many components, (2) have hierarchical structure, (3) are driven by various competing forces, and (4) interact strongly with noisy and/or nonstationary environments. It is therefore reasonable to assume that, under certain circumstances, one can analyze and interpret both physical and physiologic time series within the same framework, and that this approach could complement traditional medical diagnostics, with more precisely quantified assessments.

Quantitative analysis of physiologic time series has been a difficult and frustrating problem. The most important issues include the following:

1. The lack of proper (physical) modeling for physiologic phenomena. As a result, signals have to be considered as generated by a black box with an internal mechanism that is either poorly understood or not understood at all.
2. Signals are usually nonstationary. In other words, statistical properties of the signal may change dramatically over the observation period. Usually this change is not known *a priori* and is not explicitly advertised.
3. Usually, physiologic time series are nonlinear, revealing the nonlinear structure of various organ

Supported by Nicolet Biomedical Inc. (Madison, WI, USA) under a cooperative research and development agreement (CRADA no. 99-0559) with Oak Ridge National Laboratory. This work was also supported in part by the US Department of Energy, Office of Science, under the Laboratory Technology Research Program, and by the US Department of Energy, Office of Energy Management. V.A.P. was supported in part by the US Department of Energy, Office of Basic Energy Sciences. The Oak Ridge National Laboratory is managed for the United States Department of Energy by UT–Battelle, LLC, under contract no. DE-AC05-00OR22725.

Address correspondence and reprint requests to Dr. V. A. Protopopescu, Computer Science and Mathematics Division, Oak Ridge National Laboratory,Oak Ridge, TN, 37831-6355, USA.

dynamics and their complex, intricate interconnection, rich in feedback and hysteresis.

4. Physiologic systems rarely function at steady state. On the contrary, living processes typically occur far from equilibrium, and use continuous feedback and control to adjust to changing conditions.

One of the most important problems encountered in nonlinear time-series analysis is the appropriate characterization of features and events in complex systems' dynamics. Often these features are either described by several different quantities or do not have a precise definition at all. The former category includes (content of) information, (relative) entropy, and synchrony. Examples of the latter group are coherence, patterns, and complexity. These features may have various origins, such as nonstationarity, nonlinearity, nonequilibrium, and intertwining of length and time scales. The presence of any one of these factors frequently introduces erratic fluctuations, patchiness, lack of obvious structure, or other irregularities. Previously, these irregularities have been neglected as noise without much structure and meaning. However, recent advances in chaotic dynamics have facilitated the interpretation of intermediate and small-scale details as *bona fide* structure, with important information about the underlying dynamics. Analysis of this structure enables a deeper understanding of basic dynamic features of vital functions and organs (e.g., heart, brain, lungs), and results in more efficient assessment, prediction, prevention, control, and treatment of their malfunctions or dysfunctions.

We present a recently proposed approach for detecting dynamic change in nonlinear time series collected from scalp EEG to forewarn of impending epileptic events. We emphasize that this work is *not* a clinical analysis, but it is intended as a description and illustration of the method and its potential for event forewarning. We note that the forewarning problem is related but different from the detection of event onset (Le van Quyen et al., 1999; Osorio et al.,1998; Qu and Gotman, 1997) and event mitigation by chaos anticontrol (Schiff et al., 1994).

Epilepsy afflicts approximately 3 million people in the United States alone. Epilepsy can be treated effectively in many instances, and many patients are indeed under constant medication. However, constant medication frequently has severe side effects. Moreover, between 10% and 30% of the cases cannot be controlled by medication. In addition, some extreme events are accompanied by heart failure or breathing interruption that require immediate medical intervention. On the other hand, most events are not life threatening or even serious medical emergencies, but they represent an unpredictable source of social nuisance, disruption, and embarrassment. The possibility of robustly detecting change in EEG signals would provide quantitative means for timely clinical forewarning of impending epileptic events and would mitigate the effects of an epileptic event. Then, the patient can be forewarned to take timely preventive steps such as interrupting hazardous activities and lying down in a quiet place, taking medicine, requesting emergency responders, or contacting the physician. Consequently, a robust, reliable, and unobtrusive forewarning system would provide a new treatment paradigm whereby patients would be constantly monitored rather than continuously medicated. For outpatient and ambulatory applications, such a system should rely on *scalp* EEG alone. Although several analysis, forewarning, and/or prediction methods have been proposed and applied with various degree of success to *subdural* EEG signals, *scalp* EEG has resisted ready analysis and interpretation because of the attenuation of the meaningful signal through tissue and the high noise contamination (eye blinks, muscular tremor, involuntary movements, etc.). To detect meaningful signals through a high level of noise and artifacts, more sensitive and discriminating measures are required.

We address the forewarning problem within a purely pragmatic approach geared at designing, testing, and implementing such measures. We base this approach on a set of nested assumptions that we retain or discard by (1) Occam's razor (i.e., start with a simple explanation before resorting to a complicated one), (2) consideration of falsifiable hypotheses only, and (3) acceptance of operationally realizable tests only. In a more or less decreasing order of generality, the assumptions underlying our approach are as follows:

1. *In certain respects and under a sufficiently broad spectrum of circumstances, which includes preictal, ictal, postictal, and interictal stages, the brain behaves as a finite, dimensional, nonlinear, possibly chaotic, dynamic system*. This assumption underlies all efforts of modeling the brain by a system of coupled nonlinear (difference, ordinary differential, partial differential, and/or delay) evolution equations. In the difference or ordinary differential models, the assumption is explicit. In the other models, which are infinite dimensional, the assumption is implicit in some asymptotic sense. Indeed, such systems are infinite dimensional, but the relevant dynamics occur on a bounded, finite dimensional region of the phase space (PS), called *attractor*. To date, the validation of brain dynamics models has been attempted

only *a posteriori*, if at all. Medical and scientific literature provides evidence both for (Babloyantz and Destexhe, 1986; Elbert et al., 1994; Lerner, 1996; Pezard et al., 1994, 1996) and against (Frank et al., 1990; Gribkov and Gribkova, 2000; Ivanov et al., 1996; Jeong et al., 1999; Pradhan and Sadasivan, 1997) the description of the brain as a low-dimensional dynamic system. In our opinion, even the successful validation of *one* model would not be able—at this stage—to settle conclusively the deep and difficult questions about the nature of the brain dynamics or its accurate description. Moreover, under assumption 1, we do not attempt to answer questions about nonstationarity or nonequilibrium. Indeed, statistical tests for stationarity produce a binary result; namely, they indicate whether a change occurred, but provide no information about the extent of departure from one state to another. Stationarity tests also have limited value for inherently nonstationary processes that undergo frequent or continual changes in dynamics (e.g., physiologic data, like EEG). For such nonstationary processes, a measure of dissimilarity that quantifies the "distance" between attractors turns out to be more useful (Moeckel and Murray, 1997; Schreiber 1997, 1999).

2. *Time-serial EEG data captures the main features of nonlinear brain dynamics*. Recent studies show that different observables do not capture the same amount and/or quality of information (Letellier et al., 1998). Obviously, this feature has momentous consequences for EEG analysis.
3. The first two assumptions are easy to understand and are well documented in the literature. They warrant the *use of methods and measures for nonlinear dynamics in EEG analysis. Therefore, global aspects of brain dynamics can be adeptly captured, characterized, and discriminated by nonlinear descriptors such as Lyapunov exponents, Kolmogorov entropy, correlation dimension, and so forth* (Elbert et al., 1994). Straightforward methods exist (Abarbanel, 1996; Cover et al., 1997; Eckmann and Ruelle, 1985) for discriminating between regular and chaotic motion, or for detecting the transition between these regimes. However, distinguishing different chaotic regimes can be very difficult, especially when data are limited and noisy.
4. *PS parameters can be chosen adequately for epilepsy forewarning*. In addition to relying implicitly on the validity of assumptions 1 through 3, this assumption places constraints on the length and quality of the datasets.
5. *No notable correlation exists between the base case and the event, and thus no time relationship exists between the physiologic state of the base case and the event*. This assumption simply implies that the characteristic time of the underlying brain dynamics is much shorter than the time interval between the "normal" (base case) regime and the onset of the abnormal behavior. We see later the effect of violating this assumption on model data.
6. *A fixed threshold value for all the datasets is sufficient for robust and reliable forewarning*. On the one hand, the threshold value is easy to understand and modify operationally, but it is very difficult to justify by general principles because the very notion of threshold is "in the eye of the beholder." Conversely, the results of the analysis depend heavily on the threshold value. Continuing clinical input and adjustment is necessary for successful practical implementation.
7. *Forewarning of an event is indicated by several successive occurrences above threshold within the clinically useful forewarning window in at least one channel*. The same caveats apply to this assumption as in assumption 6. Here we choose the number of crossings by striking a balance between timeliness and accuracy of forewarning. Within the scope of this study, the judiciousness of this balance is evaluated *a posteriori*.
8. *Several simultaneous indications from the four dissimilarity measures give a reliable forewarning*. We find that the rate of false positives is minimal by requiring change indications in all dissimilarity measures.
9. *For the same patient, the same EEG channels consistently provide forewarning for one (or perhaps any) type of epilepsy*.
10. *Ideally, normal EEG data give no false positives*.

We tested systematically the validity of the assumptions 4 through 10, including various clinical checks in the algorithm development. In particular, we tested these hypotheses one by one, starting with the simplest ones via appropriate analysis of the data, while keeping the others unchanged. If an assumption was found to be false, it was rejected and replaced by a more appropriate assumption. We tested assumption 10 by applying the algorithm to both epileptic and normal (nonepileptic) EEG, as explained in Application to Scalp EEG Data. Elimination of any false positives may involve adjust-

ment of the threshold, which is one of the arbitrary parameters of our analysis. To test assumption 9 we used 41 "homogeneous" datasets for one type of epilepsy (temporal lobe [TL]) with lengths varying between 2 hours and 8 hours. This analysis determined which channels consistently give the best forewarning indications for multiple datasets from the same patient. Indeed, demonstration of consistent forewarning (or lack thereof in normal EEG) is sufficient to satisfy these criteria. Tests to date have shown that assumption 5 is invalid, because different base case periods from the same dataset give different forewarning indications in various channels. Resolution will require more analysis and understanding, perhaps involving dissimilarity comparisons of interchannel PS distribution functions (DFs) to measure neural synchrony. This analysis is necessary to clarify completely assumption 9, as well. A conclusive test of assumption 4 requires significant amounts of standard length data of verified quality for *all types* of epilepsy, together with data from healthy people. The results of such an analysis would allow a test of more "universal" values for the parameters under assumptions 5 through 10.

The following section discusses nonlinear measures for time-series analysis with special emphasis on the dissimilarity measures. The next section presents the results of our analysis first on model data and then on scalp EEG data. The last section concludes the review with a discussion of our method in comparison with other approaches.

METHODS

Nonlinear Time-Series Analysis

Nonlinear time series analysis begins with the collection of a process-indicative scalar signal, x, from a dynamic system with dimensionality, structure, parameters, and regime that are usually unknown. This signal is sampled at equal time intervals, τ, starting at the initial time, t_0, and yields a sequence of N points, $x_i = x(t_0 + i\tau)$. PS reconstruction (Eckmann and Ruelle, 1985) uses d-dimensional time-delay vectors, $y(i) = [x_i, x_{i+\lambda}, \ldots, x_i+_{(d-1)\lambda}]$, for a system with d active variables and time lag λ. The choice of lag and embedding dimension, d, determines how well the PS reconstruction unfolds the underlying dynamics from a finite amount of noisy data. Takens (1981) found that, for a d-dimensional system, $2d + 1$ dimensions generally results in a smooth, nonintersecting reconstruction. Sauer et al. (1991) showed that, using *ideal data* (i.e., no noise and infinite precision), the first integer greater than the correlation dimension is often sufficient to reconstruct the system dynamics. This result has been confirmed by computing the embedding dimension via the false nearest-neighbors method (Abarbanel and Kennel, 1993; Abarbanel et al., 1993; Cao, 1997). However, too high an embedding dimension could result in overfitting for *real data* with finite length and noise. We further note that different observables of a system contain unequal amounts of dynamic information (Letellier et al., 1998), implying that PS reconstruction could be easier from one variable, but more difficult or even next to impossible from another. As indicated in the discussion of assumptions 1 through 10, our analysis seeks to balance these caveats within the constraints imposed by the finite-length noisy data.

Various nonlinear measures have been defined to characterize process dynamics using PS reconstruction (Kantz and Schreiber, 1997; Rezek and Roberts, 1998). We choose three of these nonlinear measures, against which we compare the dissimilarity indicators. In particular, we use (1) the first minimum in the mutual information function (MIF) as a measure of decorrelation time, (2) the correlation dimension as a measure of dynamic complexity, and (3) Kolmogorov entropy as a measure of predictability. For your convenience, we briefly describe these three measures:

First, the mutual information function (MIF) is a nonlinear version of the (linear) autocorrelation and cross-correlation functions, and was developed originally by Shannon and Weaver (1949), with subsequent application to time-series analysis by Fraser and Swinney (1986). The MIF measures the average information (in bits) that can be inferred from one measurement about a subsequent measurement and is a function of the time delay between the measurements. Univariate MIF measures predictability within the same data stream at different times. Bivariate MIF measures predictability of one data channel, based on measurements in a second signal at different times. For the current analysis, we use the first minimum in the univariate MIF, M_1, to indicate the average time lag that makes x_i independent of x_j. The MIF, $I(q,r)$, and system entropy, H, are defined by

$$\mathrm{I(q, r) = I(r, q) = H(q) + H(r) - H(r, q)}, \qquad (1)$$

$$\mathrm{H(q)} = -\sum_{\mathrm{i}} \mathrm{P(q_i)log[P(q_i)]}, \qquad (2)$$

$$\mathrm{H(q, r)} = -\sum_{\mathrm{i,j}} \mathrm{P(q_i, r_j)log[P(q_i, r_j)]}. \qquad (3)$$

For a window of w points, we denote the Q set of data measurements by $q_1, q_2 \ldots, q_w$, with associated occurrence probabilities $P(q_1), P(q_2), \ldots, P(q_w)$. R denotes a

second set of data measurements, $r_1, r_2, \ldots, r_w$, with a time delay relative to the q_i values, having associated occurrence probabilities $P(r_1), P(r_2), \ldots, P(r_w)$. The function $P(q_i, r_j)$ denotes the joint probability of both states occurring simultaneously. H and I are expressed in units of bits if the logarithm is taken in base two.

Second, the maximum-likelihood correlation dimension, D, is defined by (Schouten et al., 1994a; Takens, 1984)

$$D = \{(-1/M)\sum_{ij} \ln[(\delta_{ij}/\delta_0 - \delta_n/\delta_0)/(1 - \delta_n/\delta_0)]\}^{-1}, \quad (4)$$

where M is the number of randomly sampled point pairs and δ_{ij} is the maximum-norm distance between the (randomly chosen) i–j point pairs, as defined in Eq. 6. The distance (scale length) δ_n is associated with noise as measured from the time serial data. Note that the distances are normalized with respect to a nominal scale length δ_0, which is chosen as a balance between sensitivity to local dynamics (typically at $\delta_0 \leq 5a$) and avoidance of excessive noise (typically at $\delta_0 \geq a$). Here, the symbol a denotes the absolute average deviation as a robust indicator of variability (Schouten et al., 1994a) in the time serial data

$$a = (1/w)\sum_{i=1}^{w} |x_i - \underline{x}|, \quad (5)$$

where x is the mean of x_i over the window of w points. The distances δ_{ij} are defined by

$$\delta_{ij} = \max_{0 \leq k \leq m-1} |x_{i+k} - x_{j+k}|, \quad (6)$$

where m is the average number of points per cycle.

Third, Kolmogorov entropy, K, measures the rate of information loss per unit time, or (alternatively) the degree of predictability. A positive, finite entropy is generally considered a clear demonstration that the time series and its underlying dynamics are chaotic. A very large entropy indicates a stochastic (nondeterministic) and therefore totally unpredictable phenomenon. The entropy is estimated from the average divergence time for pairs of initially close orbits. More precisely, the entropy is obtained from the average time for two points on an attractor to go from an initial separation ($\delta < \delta_0$) to a separation of more than a specific distance ($\delta > \delta_0$). The maximum-likelihood entropy is calculated from the method by Schouten et al. (1994b):

$$K = -f_s \log(1 - 1/\underline{b}), \quad (7)$$

$$\underline{b} = (1/M)\sum_{i=1}^{M} b_i, \quad (8)$$

with b_i as the number of time steps for two points, initially within $\delta < \delta_0$, to diverge to $\delta > \delta_0$. The symbol f_s denotes the data sampling rate.

There are several problems associated with the use of these measures for capturing and/or quantifying change in the dynamic regimes. The most serious is that these nonlinear measures are expressed as a sum or integral over (a region of) the PS, which averages all dynamic details into a single number. Thus, two very different dynamic regimes may lead to very close or even to equal measures. The situation is even murkier for noisy dynamics, in which case reliable determination of the nonlinear measures is next to impossible. The second difficulty is related to the fact that entropy and correlation dimension are defined in the limit of zero scale length. However, all real data have noise, and even noiseless model data are limited by the finite precision of computer arithmetic. Thus, we choose a finite scale length that is slightly larger than the noise ($\delta_0 = 2a$), at which to report the values of K and D, corresponding to finite-scale dynamic structure. Consequently, the calculated values of K and D have smaller values than expected for the zero-scale-length limit ($\delta_0 \rightarrow 0$) and cannot capture dynamic complexity at length scales smaller than δ_0. A third difficulty arises from the definition of these nonlinear measures as functionals defined on the DFs. Some of these functionals do not satisfy all the mathematic properties of a distance. In particular, for some of them symmetry and the triangle inequality may be violated (Quin Quiroga et al., 2000). Therefore, these measures cannot define a metric in the mathematic sense. They may indicate change, although only in a sense that has to be made precise for each situation.

Such limitations have led several authors to express serious doubts about the unqualified "use by transposition" of the traditional nonlinear measures for EEG data or for biologic signals in general. In an attempt to improve the discrimination power, Thomasson et al. (2001) has recently proposed the "recurrence quantification" approach that does not require assumptions about stationarity, length, or noise. Their new measure quantifies the recurrence of sets of points of various lengths that "almost repeat themselves" during the dynamics. It can be viewed somewhat as a generalization of the Poincaré section concept and is designed to detect and characterize "real phenomena" present in the EEG signal. Since we do not attempt to infer what "real phenomena" are, our approach has a much more modest goal; namely, to detect dynamic change from time series,

independent of *specific* assumptions about the underlying dynamics. As we have seen earlier, *general* assumptions *are* necessary, but—at this stage of the development of the field—we feel that they should be retained or eliminated on a minimalist and pragmatic basis alone.

Definition of the New Dissimilarity Measures

The traditional nonlinear measures described in the previous section characterize global features of the dynamics and distinguish sufficiently clearly between regular and chaotic dynamics. However, they do not reveal *slight* dissimilarities between dynamic states. The same is true for other global indicators, such as fractal dimension, Lyapunov exponents, and so forth. This lack of discrimination occurs because such traditional measures are based on averaged or integrated features of the dynamics over the attractor, which, at best, provide a global picture of long-term dynamic behavior.

Greater discrimination is possible by more detailed analysis of the reconstructed dynamics. The natural (or invariant) measure on the attractor provides a more refined representation of the reconstruction, describing the visitation frequency of the system dynamics over the PS. To obtain a useful, discrete representation of the invariant measure from time serial data, we proceed as follows. We first represent each signal value, x_i, as a symbolized form, s_i; that is, one of S different integers, $0,1, \ldots, S - 1$,

$$0 \leq s_i = \mathrm{INT}[S(x_i - x_{min})/(x_{max} - x_{min})] \leq S - 1. \qquad (9)$$

Here, the function (INT) converts a decimal number to the closest lower integer, and x_{min} and x_{max} denote the minimum and maximum values of x_i, respectively, over the base case (reference data). We previously used (Gailey et al. 1999; Hively et al. 1999, 2000b; Protopopescu et al., 2000) the minimum and maximum values over both the base case and test case (data to be tested for departure from the base case). However, in real- or near-real-time analyses, only base case extrema are actually known. We require that $s_i(x_i = x_{max}) = S - 1$ to maintain exactly S distinct symbols. Thus, the PS is partitioned into S^d hypercubes or bins. By counting the number of PS points occurring in each bin, we obtain the DF as a "discretized" density on the attractor. We denote the population of the ith bin of the DF, Q_i, for the base case, and R_i for a test case respectively. For infinitely precise data, this representation has been used in Grebogi et al. (1988). The choice of parameters (S, N, and d) depends not only on the system, but also on the specific data under consideration. During the preliminary phase of the analysis, we systematically varied each parameter with the others fixed, to obtain optimum sensitivity of the measures to changes in system dynamics for each class of data evaluated. After realizing optimal sensitivity, the values of the parameters were kept fixed.

We use an embedding window, $M_1 = (d - 1)\lambda$, based on the first minimum in the MIF, M_1 (Fraser and Swinney, 1986). This choice of time delay provides maximal information for the reconstruction of the PS dynamics. Then, we set $\lambda = \mathrm{INT}[0.5 + M_1/(d - 1)]$ to obtain an integer value for the reconstruction lag when M_1 is not evenly divisible by $d - 1$. The reconstruction requires that $\lambda \geq 1$, thus constraining the largest value of dimensionality to $d \leq 2M_1 + 1$ from the previous formula.

Once the dynamics is reconstructed (unfolded), the test case is compared with the base case. Diks et al. (1996) measured differences between delay vector distributions by the square of the distance between two DFs. Schreiber (1997, 1999) measured dissimilarity via the Euclidean distance between points of the attractor. This measure *only* accounts for the geometric shape and location of the attractor. Manuca and Savit (1996) and Manuca et al. (1998) described dissimilarity via ratios of the correlation integral over the DF. This is essentially the correlation dimension discussed in the previous section. Moreover, these papers discuss dissimilarity measures from the perspective of nonstationarity, whereas our focus is on condition change, as explained earlier. We measure the difference between Q_i with R_i by the χ^2 statistic and L_1 distance:

$$\chi^2 = \sum_i (Q_i - R_i)^2/(Q_i + R_i), \qquad (10)$$

$$L = \sum_i |Q_i - R_i|, \qquad (11)$$

where the summations in both equations run over all the populated PS cells. The choice of these measures is based on the following considerations. The χ^2 statistic is one of the most powerful, robust, and widely used *statistical* tests to measure discrepancies between observed and expected frequencies. The χ^2 statistic is obviously symmetric, but does not always satisfy the triangle inequality, so it does not define a distance in the mathematic sense. The L_1 distance is the natural metric for distribution functions because it is directly related to the total invariant measure on the attractor and does define a *bona fide* distance. Therefore, these measures account for changes in the geometry, shape, and visitation frequency of the attractor, and can be viewed as somewhat complementary. Obviously, calculation of these measures in a consistent fashion requires that the base case and test case contain the same number of

points, identically sampled; otherwise, the DFs have to be rescaled properly.

We extended the previous analysis in a manner that is naturally compatible with the underlying dynamics. By connecting successive PS points as prescribed by the dynamics $y(i) \rightarrow y(i+1)$, $i = 1,2,\ldots$, we obtained a discrete representation of the process flow (Abarbanel, 1996). The $2d$-dimensional vector, $Y(i) = [y(i), y(i+1)]$, formed by adjoining two successive vectors from the d-dimensional reconstructed PS, lives in a $2d$-dimensional space, that we call the connected phase space (CPS). As before, Q and R denote the CPS DFs for the base case and test case respectively. We define the measures of dissimilarity between these two CPS DFs, as before, via the L_1 distance and the χ^2 statistic, (Hively et al., 1999, 2000b):

$$\chi_c^2 = \sum_{ij} |Q_{ij} - R_{ij}|^2/(Q_{ij} + R_{ij}) \tag{12}$$

$$L_c = \sum_{ij} |Q_{ij} - R_{ij}|. \tag{13}$$

The subscript c indicates the connected DF measure. We note that the value $\lambda = 1$ results in $d - 1$ components of $y(i+1)$ being redundant with those of $y(i)$, but we allow for this redundancy to accommodate other data such as discrete points from two-dimensional maps. The CPS measures have a higher discriminating power than their nonconnected counterparts. Indeed, we can prove that the measures defined in Eqs. 10 through 13 satisfy the following inequalities: $\chi^2 \leq L$, $\chi_c^2 \leq L_c$, $L \leq L_c$, and $\chi^2 \leq \chi_c^2$ (Hively et al., 2000b).

Use of the χ^2 statistic requires statistical independence between various samples. However, the PS points depend on one another as a result of reconstruction from time delay vectors with dynamic structure (Diks et al., 1996). The resulting statistical bias is avoidable by averaging contributions to Eqs. 10 and 12 over values of $y(j)$ or $Y(j)$, which satisfy $|i - j| < \Lambda$ (Diks et al., 1996), where Λ is some largest typical correlation scale length in the time series. We tested the bias in typical data by sampling every Λ-th CPS point for $4 \leq \Lambda \leq 23$, resulting in Λ different samples for the base case (Q_i) and for each cut set (R_i). We then averaged the sampled χ^2 values over the Λ^2 different combinations of distribution functions for the base case and test case cut sets. As expected, a decrease proportional to $1/\Lambda$ occurs in the sampled χ^2 values, because the number of data points contributing to χ^2 decreases in the same proportion. The trend over time in sampled χ^2 values remains the same as in χ^2 values without sampling, showing that no bias is present. Thus, we use unsampled χ^2 values for the remainder of this work as a *relative* measure, rather than as an unbiased χ^2 statistic for accepting or rejecting a null statistical hypothesis. (Hively et al., 1999).

Use of the dissimilarity measures on finite-length, noisy data requires a consistent statistical implementation and interpretation. Moreover, construction of the base cases also requires careful statistics to eliminate possible outliers and to ensure robust results. We use the first N nonoverlapping cut sets in each of the datasets as base cases. For each dataset, the choice of N should strike a judicious balance between a reasonably short base case period to capture quasistationary, "normal" dynamics and a sufficiently long period for significance. However, a few of these base case cut sets may be very different from the typical regime, causing a severe bias in the detection of condition change. This is especially true for noisy physiologic data. We statistically test the base case cut sets for outliers as follows. Dissimilarity comparisons among the N base case cut sets yields $N(N-1)/2$ unique pairs, from which we obtain an average, $\underline{V}$, and sample standard deviation, σ, for each of the dissimilarity measures, $V = L$, L_c, χ^2, and $\chi_c{}^2$. We calculate a χ^2 statistic, $\Sigma(V_{ij} - \underline{V})^2/\sigma$, for each of these four dissimilarity measures. The index j is fixed, to test the jth cut set against the other $N - 1$ cut sets, thereby giving $N - 1$ degrees of freedom in the χ^2 statistic. The null statistical hypothesis allows a random outlier with a probability less than $2/N(N-1)$, corresponding to less than one out of the $N(N-1)/2$ unique pairs. We have chosen $N = 5$ for the noiseless model-generated data, where, for fixed dynamic conditions, the variability arises only from the location in and the discrete sampling of the PS. On the other hand, for noisy EEG data we have chosen $N = 10$, to provide a larger statistical sample.

In the latter case, we identify an outlier cut set as having the largest χ^2 statistic greater than 19.38 over the four dissimilarity measures, which corresponds to a probability larger than 1/45. If this analysis does not identify any outlier, then the previous values of V are used for subsequent renormalization, as described later. If this analysis identifies an outlier, we remove it. We then repeat this analysis for the remaining nine base case cut sets to identify any additional outliers when the largest χ^2 statistic exceeds the threshold, corresponding to a random probability of more than $2/B(B-1)$, as interpolated from standard statistical tables for $B - 1$ degrees of freedom (Abramowitz and Stegun, 1964). Here, B is the number of nonoutlier base case cut sets. Thus, rejection of the null hypothesis corresponds to a χ^2

statistic more than 19.38, 17.24, 15.03, 12.74, and 10.33, for $B = 10$, 9, 8, 7, and 6, respectively.

This approach improves dramatically the robustness of the condition change detection. If the analysis identifies five (or more) outliers, we would have to reject all 10 base cases as unrepresentative, and acquire a new set of 10 cut sets as base cases. However, the current analysis never finds more than four outliers. Subsequently, we compare the nonoutlier base case cut sets with each nonoverlapping test case cut set, and obtain average values for the dissimilarity measures for each test case.

The disparate range and variability of the various nonlinear measures are difficult to interpret (especially for noisy data), so we need a consistent means of comparison. Thus, we convert the nonlinear measures to a renormalized form (Hively et al., 1999, 2000b). For each nonlinear measure, $V = \{D, K, M_1, L, L_c, \chi^2$, and $\chi_c{}^2\}$, we define V_i as the value of the nonlinear measure for the ith cut set. As before, $\underline{V}$ is the mean value of that nonlinear measure over the nonoutlier base cases, with a corresponding sample standard deviation σ, as described earlier. No such averaging is done for D, K, and M_1 because the calculation of these measures involves only one cut set at the time. The renormalized form is then $U(V) = |V_i - \underline{V}|/\sigma$, which measures the number of standard deviations that the test case deviates from the base case mean. For a positive indication of change in EEG (see Application to Scalp EEG Data), we require N_{occ} successive occurrences above the threshold, $U \geq U_{crit}$.

RESULTS

Application to Model Data

We assessed the discriminating power of the nonlinear measures by first testing them as well as some of the assumptions 1 through 10 on noiseless model-generated time-serial data. We considered the well-known Lorenz model (Lorenz, 1963) that is a three-dimensional system of coupled, nonlinear differential equations:

$$\frac{dx}{dt} = a(y - x), \frac{dy}{dt} = rx - y - xz, \frac{dz}{dt} = xy - bz \quad (14)$$

with properties that have been well documented in the literature. We integrated the Lorenz system with time steps $\delta t = 0.03$ and used the variable y to reconstruct the dynamics. We fixed parameters a and b at the values 10 and 8/3 respectively. As the variable parameter r increases from zero, the solutions the Lorenz system displays increased complexity and different stability properties. Transitions from one type of solution to another occur through bifurcations or transitions to chaos for which traditional nonlinear measures are, in general, good indicators. However transitions between two chaotic regimes are not readily detected by these traditional measures, especially for small changes in the parameter r. Therefore, we concentrate on detecting dynamic change within a region where the Lorenz system behaves chaotically (Jackson, 1989, 1990); namely, for $45 \leq r \leq 90$. We started with $r = 45$, which was considered the base case, and kept r unchanged for 2,250,000 points (45 cut sets of 50,000 points). Then we increased r from 45 to 90 in one-unit steps for each 50,000-point window. Finally, we maintained $r = 90$ for another 2,250,000 points (45 cut sets of 50,000 points). Fig. 1 shows the consistency and robustness of the resulting dissimilarity measures. Indeed, as long as the parameter r is unchanged, the dynamic system remains in the same regime, and the dissimilarity measures remain consistently close to zero. When the parameter varies monotonically, the dissimilarity measures increase monotonically, in roughly linear fashion, and over a much broader range than the traditional nonlinear measures. The dissimilarity measures reach a clear plateau at $r = 90$, illustrating their consistency. Here the base case consisted of the first 10 adjacent windows for $r = 45$. We obtained the traditional and (C)PS renormalized measures by comparing the distribution function for each 50,000-point test case to each of the 10 base cases using Eqs. 10 through 13. We note that the CPS measures (dashed curves in Fig. 1) lie below the nonconnected measures (solid curves in Fig. 1). This does not contradict the theoretic results (Hively et al., 2000b), because the curves in Fig. 1 were obtained by averaging, to obtain renormalized measures. Only the MIF values are given in the unrenormalized form because the first minimum in the MIF is completely constant over the base case, resulting in $\sigma = 0$. Of course, if the window length decreases, more variability appears and σ would be different from zero. Fig. 1 shows various nonlinear measures versus r. The correlation dimension (Fig. 1A) varies erratically between 0 and 0.2 over the whole range. The renormalized Kolmogorov entropy (Fig. 1B) also varies erratically while gradually rising from 0 to 4. Fig. 1C shows the location of the first minimum in the mutual information function, M_1, with a single abrupt step at $r = 60$. A smaller integration step ($\delta t = 0.1$) yields a series of finer steps (not shown here), thereby illustrating the limitation of a coarser sampling rate. In sharp contrast, the (C)PS measures (Figs. 1D, E) increase almost monotonically from zero to more than 500 as r increases from 45 to 90. The values of L and χ^2 essentially coincide over the whole range because the

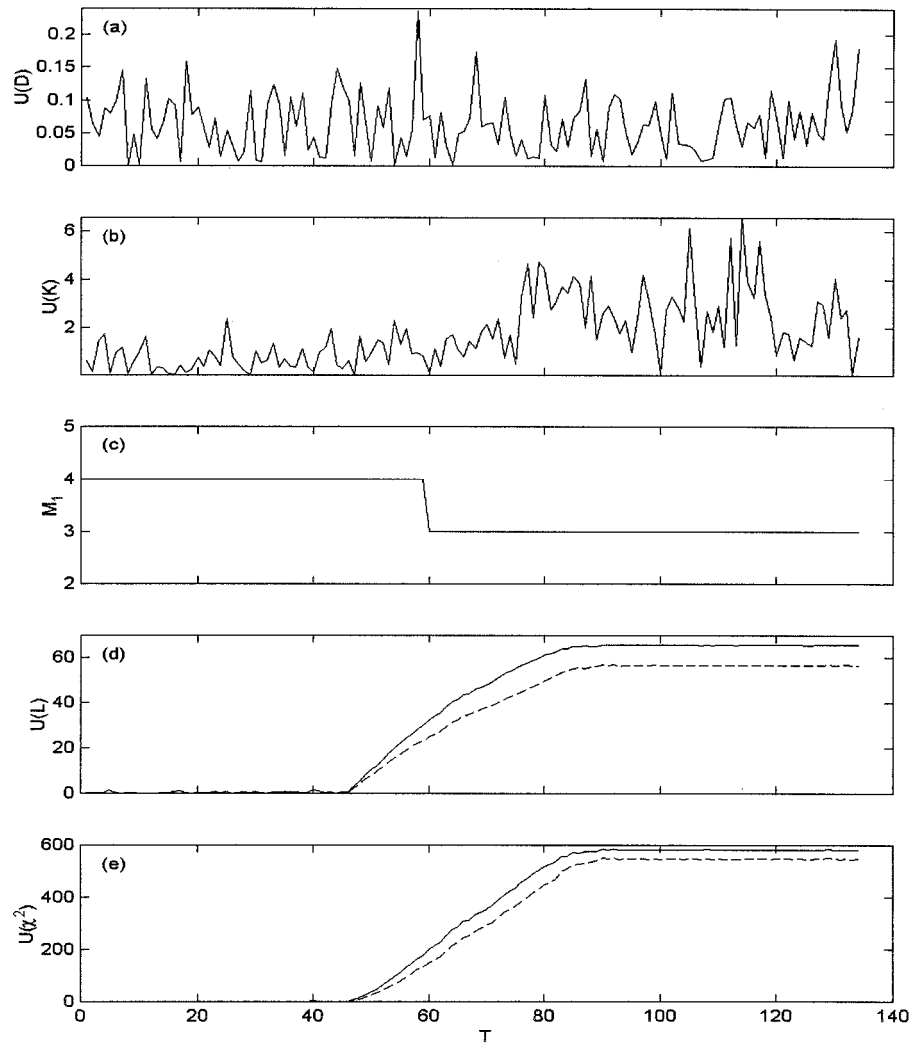

FIG. 1. Renormalized nonlinear measure versus r calculated from the y variable of the Lorenz system: **(a)** correlation dimension, **(b)** Kolmogorov entropy, **(c)** lag (in time steps) of the first minimum in the mutual information function, **(d)** non-connected (solid) and connected (–) L_1 dissimilarity, and **(e)** non-connected (solid) and connected (–) χ^2 dissimilarity. The phase-space reconstruction parameters are: S=12, d=3, N=50,000, and λ = 2. No variability occurs in the values of M_1 for r=45, so subplot (c) is not renormalized. The value of r is as follows: r=45 for $0 \leq T \leq 45$, r=T for $46 \leq T \leq 89$, r=90 for $90 \leq T \leq 134$.

measures are dominated by PS bins that are populated only for the base case ($Q_i > 0$ for $R_i = 0$) and only the test case ($R_i > 0$ for $Q_i = 0$), for which the two measures become analytically equivalent. Fig. 2 shows the dissimilarity measures for a different choice of the base case; namely, over the first 10 cut sets of $r = 90$. These curves are roughly mirror images of those in Fig. 1: large and constant dissimilarity for $r = 45$; a monotonic, approximately linear decrease during the transition ($45 < r < 90$); and small dissimilarity in the base case region ($r = 90$). Fig. 3 shows the dissimilarity measures for several lengths of the window, varying from 5,000 to 25 points. As expected, the quality of the results degrades dramatically as the length of the window shortens. For a very short window, the long-range regularity of the dynamics is overcome by short-range variability, which depends substantially on the specific location in the PS. This result underscores the importance of the relationship between the length of the dataset, the characteristic times of the underlying dynamics, and the need for "sufficiently long datasets" for "sufficiently good" statistics.

In addition to the Lorenz system, we assessed the discriminating power of the dissimilarity measures on the Bondarenko "synthetic brain" model (Bondarenko, 1997). The interest in this model is twofold: On the one hand, it is supposed to mimic well the general features of actual EEG signals; on the other hand, and unlike the Lorenz system, it is an infinite dimensional model described by a system of time-delayed, ordinary differential equations:

$$\frac{du_i(t)}{dt} = -u_i(t) + \sum_{i=j}^{M} a_{ij} f(u_j(t - \tau_j)), \quad i, j = 1, 2, ..., M. \tag{15}$$

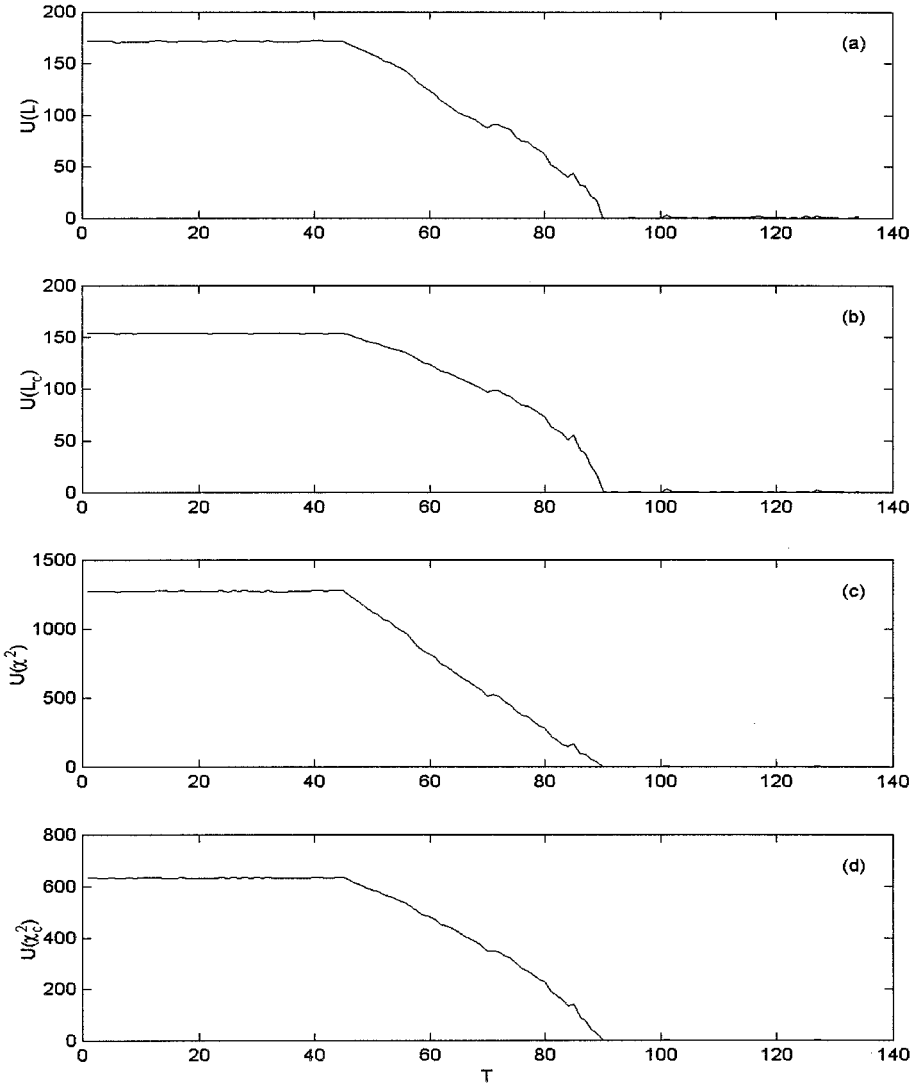

FIG. 2. Renormalized nonlinear measures versus r calculated from the y variable of the Lorenz system with the basecase over the first 10 cutsets of $r=90$: **(a)** non-connected L_1 dissimilarity, **(b)** connected L_1 dissimilarity, **(c)** non-connected connected χ^2 dissimilarity, and **(d)** connected χ^2 dissimilarity. The phase-space reconstruction parameters are: $S=12$, $d=3$, $N=50{,}000$, and $\lambda = 7$. The value of r is as follows: $r=45$ for $0 \leq T \leq 45$, $r=T$ for $46 \leq T \leq 89$, $r=90$ for $90 \leq T \leq 134$.

Eq. 15 is obtained from the finite-dimensional Hopfield model for the electronic circuit realization of a neural network by adding a time delay τ_j. Here, $u_i(t)$ is the output signal of the ith neuron and the matrix a_{ij} denotes the coupling coefficients between the neurons, with randomly chosen values, $-2 \leq a_{ij} \leq 2$. For this particular implementation, the indices i and j run from 1 to $M = 10$ (10 neurons). The time delay of the jth neuron output, τ_j, is constant and equal to 10. The nonlinear response function, $f(x) = c \tanh(x)$, simulates the nonlinear neural response to signals from neighboring neurons. We vary the coefficient c to change the values of the coupling coefficients between the neurons a_{ij} simultaneously.

As discussed earlier, the traditional nonlinear measures are good indicators of either bifurcations or transitions to chaos. However, transitions between two chaotic regimes are not readily detected by these same measures, especially for relatively small changes in the parameter that underlies the transition. Therefore, the current work concentrates on measuring dissimilarity within a region where the Bondarenko system is known to behave chaotically; namely, $5 \leq c \leq 18$ (Bondarenko, 1997). The model was integrated by using a standard fourth-order Runge–Kutta method with a time step equal to 0.3. We allowed 40,000 time steps for the solution to achieve stationarity after initiating the integration with random impulses, $u_j(t = 0) = \rho_j$ for uniformly random values, $-2 \leq \rho_j \leq 2$. We calculated 100,000 data values of u_i at fixed time intervals of $\Delta t = 10$ for each value of c. We obtained the (C)PS measures by partitioning each 100,000-point Bondarenko dataset into five nonoverlap-

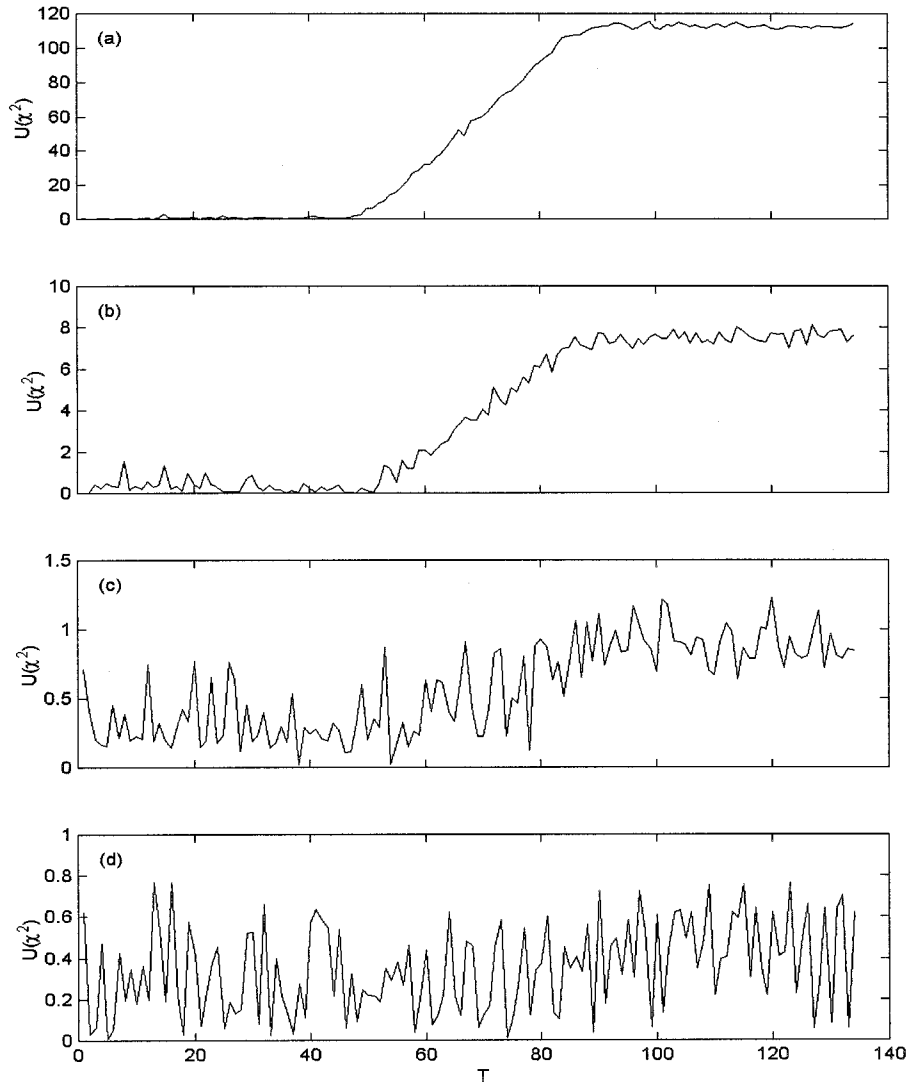

FIG. 3. Renormalized nonlinear measures versus r calculated from the y variable of the Lorenz system: **(a)** non-connected χ^2 dissimilarity for $N=5000$, **(b)** non-connected χ^2 dissimilarity for $N=500$, **(c)** non-connected χ^2 dissimilarity for $N=50$, **(d)** non-connected χ^2 dissimilarity for $N=25$. The phase-space reconstruction parameters are: $S=12$, $d=3$, and $\lambda = 2$. The value of r is as follows: $r=45$ for $0 \leq T \leq 45$, $r=T$ for $46 \leq T \leq 89$, $r=90$ for $90 \leq T \leq 134$.

ping subsets of 20,000 points each, for comparison with each of the 20,000-point subsets of base case at $c = 5$.

Fig. 4 shows various renormalized nonlinear measures versus c, by analyzing only the signal from one neuron of the Bondarenko system. Here (unlike the Lorenz system), we obtain similar results when other neuron signals are used to reconstruct the dynamics. The renormalized correlation dimension (Fig. 4a) varies erratically between 0 and 0.1. The renormalized Kolmogorov entropy (Fig. 4b) increases erratically from 0 to approximately 2.0. Fig. 4c shows the renormalized location of the first minimum in the MIF, M_1, with erratic variation between 0 and 0.1, as c increases. In sharp contrast, the (C)PS measures (Figs. 4d, e) increase almost monotonically from zero to more than 40, as c increases from 5 to 18. Note that the CPS measures are stronger than their nonconnected counterparts.

Application to Scalp EEG Data

We turn next to analysis of brain wave data. Nonlinear EEG measures are not stationary, displaying instead marked transitions between normal and epileptic states (Manuca and Savit, 1996; Manuca et al., 1998). As established by many authors, EEG data seem to display low-dimensional features (Elbert et al., 1994; Lehnertz and Elger, 1998) with at least one positive Lyapunov exponent (Elbert et al., 1994; Iasemidis and Sackellares, 1991, 1996), and hence positive Kolmogorov entropy. EEG data also display clear PS structure (Elbert et al.,

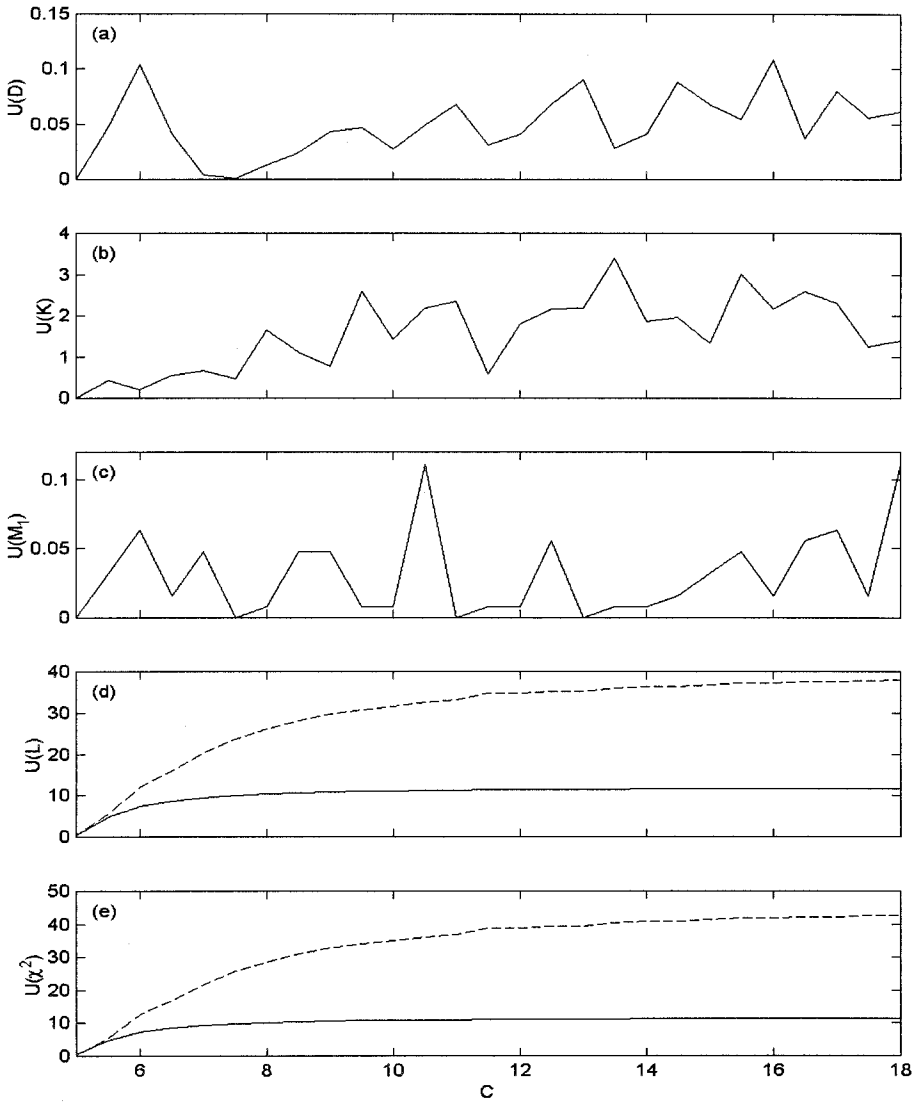

FIG. 4. Renormalized nonlinear measures versus c calculated from one neuron channel of the Bondarenko system: **(a)** correlation dimension, **(b)** Kolmogorov entropy, **(c)** lag (in time steps) of the first minimum in the mutual information function, **(d)** non-connected (solid) and connected (–) L_1 dissimilarity, and **(e)** non-connected (solid) and connected (–) χ^2 dissimilarity. The phase-space reconstruction parameters are: S=34, d=3, N=20,000, and λ = 13.

1994; Iasemidis and Sackellares, 1996), on which our analysis relies for measuring condition change. We find that PS measures are useful for nonlinear detection of condition changes in brain wave data (Hively et al., 1999, 2000a and 2000b). We emphasize that our work relies on scalp EEG, which measures the noisy synchronous dynamics in cortical neurons over an area of roughly 6 cm^2 as attenuated through the skull. Our analysis assumes that both the traditional and the new measures are sensitive to changes in nonlinear dynamics (Elbert et al., 1994).

Recordings came from 32-channel Biomedical Monitoring Systems Inc. instruments (Nicolet-BMSI, Madison, WI, USA) with 19 scalp electrodes in the International 10-20 System of placement as referenced to the ear on the opposing hemisphere. Each channel of scalp potential was amplified separately, bandpass filtered between 0.5 to 99 Hz, and digitized at 250 Hz.

We analyzed 41 datasets with at least one electrographic temporal lobe (TL) event, broken down further by clinical event type in Table 1. We analyzed 20 additional datasets without TL events as controls. This work was performed in accord with the United Status National Institutes of Health Human Studies Review guidelines, although internal review board approval is not required for this privately funded research. In particular, physicians obtained the EEG data with informed consent of the patients or their guardians, under standard protocols for epilepsy unit monitoring. We ensured patient anonymity by using only numeric identifiers. The

TABLE 1. *Characterization of datasets*

PID	DID	S	AG	START	STOP	T (EV)			AE		TYP	B-ACT	E-ACT
3	12	F	15	23:30	03:54	03:24					P		
4	13	F	44	07:56	11:58	11:28					P	OOC, eating	Reading
5	16	M	7	03:54	08:50	08:20					P	Asleep	LIB, TV, eating
99	17	F	17	12:22	14:20						NE	Awake	
6	18	M	43	10:39	13:57	13:26					G	NVOV	Asleep
6	19	M	43	16:34	20:40	20:10					G	Asleep	Asleep
7	20	F	12	19:40	23:18	22:48			T3		P	Eating, talking	Asleep
100	22	M	21	11:45	13:50						NE	Awake	
8	24	M	30	21:24	01:09	00:39					P2G	LIB, talking	EC, LIB, talking
8	26	M	30	03:13	06:25	06:55					NS	Seizure, asleep	Asleep
11	37	F	42	19:29	01:18	01:29					NS		LIB (lights off)
11	39	F	42	15:16	20:18	19:48					P	Asleep, TV	LIB, FIDG, reading
12	42	M	34	04:55	09:17	08:47					P	Asleep, awake, NVOV	Eating, talking
12	46	M	34	10:23	14:03	13:33					P	Talking, TV, LIB	Talking, SIB
11	125	F	42	14:17	19:56	19:13	19:25				P2G	TV, talking	GU, NVOV, FIDG
19	127	M	4	01:04	04:49	04:10			T3		NS	Asleep	Awake, SIB, LIB
19	129	M	4	14:37	17:59	15:22	16:25	17:29	T3		P2G	Asleep	Reading, talking
11	131	F	42	14:08	19:30	19:01					P	SIB, TV	TV, LOM
22	149	F	43	07:22	09:12	08:22					NE		
22	150	F	43	09:51	11:52	11:24					NE		
24	157	F	41	02:23	04:24	03:36					NE		
24	158	F	41	21:44	23:36	23:09					NE		
24	163	F	41	18:12	19:36						NS		
24	165	F	41	12:36	15:59						NS		
27	170	M	37	11:05	14:04	14:02			F7		P		
75	193	M	41	09:41	12:45	12:39			T3		P		
81	199	M	41	00:36	06:53	06:45			T3		P	Asleep	GU, NVOV, FIDG
82	200	M	23	16:12	20:40	19:59			F3	F4	G	SIB, PWAT	SIB, PWAT, SPAC
84	203	F	33	00:05	05:44	05:42			T3		P2G	Reading	Asleep
83	207	F	33	08:06	15:17	14:42			T3		P	Reading, talking	Asleep
86	211	M	41	18:41	23:59	23:52			T3		P2G	SIB	Asleep
74	214	F	32	18:54	23:50	23:45			T3		P	Asleep	Awake, TV
74	216	F	32	04:15	07:11	06:59			T3		P	Asleep	Awake LIB/RA GU
89	222	F	52	10:47	15:02	13:23	13:29	14:27	T3		P	WWN	SIB, talking, BP
90	221	M	43	16:03	19:49	19:19			T3		P	LIB, talking, EC	SIB, eating
40	235	F	51	20:54	02:42	02:33			T4		P2G	SIC, TV	SIB, talking (SPAC)
46	255	F	16	21:09	00:51	00:49			T3		P	Asleep	
47	259	F	43	11:54	14:47	14:44					P	LIB, talking, eating	NVOV, LIB/VW
48	261	F	14	16:11	21:17	21:02					NS	LIB, TV	LIB (LOM)
61	264	M	33	07:50	11:14	11:09			T3		P		
61	265	M	33	23:47	06:33	06:29			T3		P	TV, eating, drinking	Asleep
61	266	M	33	07:45	11:55	11:52			T3		P	NVOV	SOSB
61	267	M	33	07:43	10:45	10:38			T3		P	SOSB, talking	Asleep
62	270	F	27	15:46	17:23	15:49					NE		
61	271	M	33	07:45	12:11	11:57			T3		P	SIB, drinking, TV	Talking, SIB
63	273	F	44	07:44	14:59	10:31	11:04	14:54			NE	Eating, talking	SIC, talking, yawning
64	274	F	56	07:38	09:04	08:28					NE		
64	275	F	56	07:37	13:00	12:09					NE	Drinking	NVOV
64	276	F	56	05:13	11:38	11:45					NE	SOSB, rocking	NVOV
67	283	F	20	11:38	15:07	14:32					NE	Talking	Breathing hard
65	284	M	58	07:51	13:25	13:11					NS	LIB, LOOK (SPAC)	SIB, TV
67	285	F	20	15:44	20:35	19:46					NE	Awake, SIB	LIB, EC
68	286	M	56	23:40	04:11	03:32			T3		P2G	Asleep, (LOM)	Asleep
66	287	M	19	10:00	17:28	12:47	17:49				P	TV	Talking
69	289	F	57	16:38	22:34	21:38			T4		P	Talking, NVOV	Asleep
70	293	F	44	20:38	00:38	00:31					P	TV, talking, laughing	LIB, writing CARD
69	299	F	57	23:56	03:21	03:19			T4		P	TV, EC	Asleep
72	300	F	44	23:41	05:11	04:51			T3		P	Asleep	Asleep
94	308	F	15	08:14	11:56	11:52			T4		P		
30	386	F	15	05:57	10:49	09:04	09:57		F7	T3	P		
54	403	M	12	02:56	08:02	08:00					P		

There was a total of 46 temporal lobe (TL) events (22 female and 24 male patients) from 33 different patients with the following distribution of event types: partial (n = 31), partial secondarily generalized (n = 7), generalized (n = 3), and nonseizure (n = 5).

There was a total of 17 nonepileptic or nonseizure events datasets (16 female patients and 1 male patient).

Patient 64 had a left temporal lobe resection with new, nonepileptic episodes. EEG was read by as "normal" during the episodes.

PID, patient identifier; DID, dataset identifier; S, sex of patient; M, male; F, female; AG, age of patient (years); START, starting time of dataset (hh:mm); STOP, stoping time of dataset (hh:mm); T (EV), time of TL events (hh:mm) accounting for multiple events; AE, active electrode; TYP, type; P, partial; NE, non event; NS, nonseizure; G, generalized; P2G, partial secondarily generalized; TYP, type; B-ACT, activity during base case period; E-ACT, activity immediately before event; BP, blood pressure checked; CARD, plays cards; EC, eyes closed; FIDG, fidgeting; GU, got up (out of sight); LIB, lying in bed; LOM, lots of movement; LOOK, looking around; NVOV, not visible on video; OOC, out of chair; PWAT, playing with a toy; RA, rolling around; SIB, sitting in bed; SIC, sitting in chair; SOSB, sitting on side of bed; SPAC, spacey; TV, watching TV; VW, very wiggly; WWN, working with nurse.

TABLE 2. *Summary of forewarning analysis*

				Forewarning time (sec) by channel																		
PID	DID	T(SZ)	T(EN)	FP1	FP2	F3	F4	C3	C4	P3	P4	O1	O2	F7	F8	T3	T4	T5	T6	FZ	CZ	PZ
3	12	14040	15750	FP	FP	FP	FP	3040	FP	FP	FP	FP	FP	FP	FP	FP	FN	FP	FP	FP	FP	FP
4	13	12720	14500	FP	720	FP	FP	FN	FP	FP	FN	FP	FP	FP	FP	FP	FN	FN	FN	FN	FN	FN
5	16	15960	17750	FP	FP	FP	FP	FP	2460	FP	FP	FP	FP	FP	FP	3460	FP	FP	FP	FP	FP	FP
6	18	10020	11750	FN	FN	FN	FP	FN	770	FN	FN	FN	FN	FN	FN	FP	270	FN	FN	FN	FN	FN
6	19	12960	14750	FN	FP	FN	FN	FN	FN	FN	FP	1460	FP	FP	FN	FP	FP	FN	1960	1710	3210	FP
7	20	11280	13000	FN	FN	FP	FN	FN	FN	FP	1780	530	FN	FN	280	1780	FN	FN	1280	FN	FP	FP
8	24	11700	13500	FP	950	FP	FP	FP	FP	FP	FP	FP	FP	FP	FP	FP	FP	FP	FP	FP	FP	FP
8	26	0	13250	TN	TN	TN	TN	TN	TN	TN	TN	TN	TN	TN	TN	TN	TN	TN	TN	TN	TN	TN
11	37	0	23000	TN	TN	TN	TN	TN	TN	TN	TN	TN	TN	TN	TN	TN	TN	TN	TN	TN	TN	TN
11	39	16320	16500	820	FN	FP	FN	FP	FP	FP	FP	FN	FP	FP	FP	FP	FP	FP	FP	FP	FN	FP
11	125	17760	20250	FN	FP	FN	FP	FN	FP	3010	FP	FP	FP	FP	FN	FP	FN	FP	260	FP	FP	FP
11	131	17580	19250	3580	FP	FP	FP	FP	FN	FP	FN	FN	FN	FN	FP	FP	1330	FP	FP	FP	FP	FN
12	42	13920	11500	FP	2920	FP	FP	2920	FP	2920	FP	FP	3170	FP	FP	FP	FP	FP	FP	FP	3420	FN
12	46	11400	13000	FN	FP	FP	FP	FP	FP	1650	FP	FP	FP	FN	FN	FP	FN	FP	1150	FN	650	1150
19	127	0	21000	TN	TN	TN	TN	TN	TN	TN	TN	TN	TN	TN	TN	TN	TN	TN	TN	TN	TN	TN
22	149	0	6500	TN	TN	TN	TN	TN	TN	TN	TN	TN	TN	TN	TN	TN	TN	TN	TN	TN	TN	TN
22	150	0	7250	TN	TN	TN	TN	TN	TN	TN	TN	TN	TN	TN	TN	TN	TN	TN	TN	TN	TN	TN
24	157	0	7250	TN	TN	TN	TN	TN	TN	TN	TN	TN	TN	TN	TN	TN	TN	TN	TN	TN	TN	TN
24	158	0	6500	TN	TN	TN	TN	TN	TN	TN	TN	TN	TN	TN	TN	TN	TN	TN	TN	TN	TN	TN
24	163	0	5000	TN	TN	TN	TN	TN	TN	TN	TN	TN	TN	TN	TN	TN	TN	TN	TN	TN	TN	TN
24	165	0	12000	TN	TN	TN	TN	TN	TN	TN	TN	TN	TN	TN	TN	TN	TN	TN	TN	TN	TN	TN
27	170	10620	10500	FP	FP	1370	FP	FP	FN	FP	FN	1870	FP	FP	2620	FP	FN	FP	FP	FP	1120	FP
30	386	11220	18250	FP	FP	FP	220	FP	1720	FP	1470	2720	FP	FP	FP	FN	FP	FP	1470	FP	3220	FN
40	235	20340	20750	FP	FP	FP	FP	2590	FP	FP	FP	FP	3340	FP	FP	FP	3340	FP	FP	FP	FP	FP
46	255	13200	13250	FP	FP	FP	FP	FP	FP	FP	FP	FP	FP	FP	FN	FN	FP	450	FP	FP	3200	FP
47	259	10200	10250	FP	FN	FP	FN	FP	FN	FP	3450	2950	FP	2950	FP	2200	FP	FP	FN	2200	FP	FP
48	261	0	19250	TN	TN	TN	TN	TN	TN	TN	TN	TN	TN	TN	TN	TN	TN	TN	TN	TN	TN	TN
54	403	18240	18750	FP	1490	1490	FP	FP	1240	1240	FP	1740	FP	FP	FP	FP	FN	1240	FP	FP	FP	1990
61	264	11940	12000	1690	3440	2440	3440	1940	FN	FP	FP	2440	2940	FN	FP	FP	FP	FP	FP	FN	FP	FP
61	265	24120	24250	FP	FP	FP	2870	FP	FP	FP	FP	FP	FN	FP	FN	FN	FN	FP	FP	FP	FP	FP
61	266	14820	15250	1820	2570	FN	FP	3570	FP	FP	FP	FP	FN	FP	1570	FN	70	FN	FN	FP	3320	FP
61	267	10500	10750	FP	FN	FP	FN	FN	FN	FN	1500	FP	FN	FN	FN	FN	FN	FN	FP	FP	1500	2500
61	271	15120	15750	FP	1370	FP	FP	FP	FP	FP	FP	FP	FP	FP	FN	FP	FP	FP	2870	620	FN	FP
62	270	0	5750	TN	TN	TN	TN	TN	TN	TN	TN	TN	TN	TN	TN	TN	TN	TN	TN	TN	TN	TN
63	273	0	26000	TN	TN	TN	TN	TN	TN	TN	TN	TN	TN	TN	TN	TN	TN	TN	TN	TN	TN	TN
64	274	0	5000	TN	TN	TN	TN	TN	TN	TN	TN	TN	TN	TN	TN	TN	TN	TN	TN	TN	TN	TN
64	275	0	19250	TN	TN	TN	TN	TN	TN	TN	TN	TN	TN	TN	TN	TN	TN	TN	TN	TN	TN	TN
64	276	0	23000	TN	TN	TN	TN	TN	TN	TN	TN	TN	TN	TN	TN	TN	TN	TN	TN	TN	TN	TN
65	284	0	20750	TN	TN	TN	TN	TN	TN	TN	TN	TN	TN	TN	TN	TN	TN	TN	TN	TN	TN	TN
66	287	10020	27250	FP	FP	2020	FP	FP	FP	FP	FP	FP	FP	FN	FP	FP	FN	FP	3520	FN	3020	FP
67	283	0	12750	TN	TN	TN	TN	TN	TN	TN	TN	TN	TN	TN	TN	TN	TN	TN	TN	TN	TN	TN
67	285	0	17250	TN	TN	TN	TN	TN	TN	TN	TN	TN	TN	TN	TN	TN	TN	TN	TN	TN	TN	TN
68	286	13920	16250	FP	FP	FN	FP	FN	FN	FN	FN	FN	FP	FN	FP	FN	FN	FP	FP	FP	FP	FN
69	289	18000	21250	FP	FP	FP	FP	FP	FP	FP	FP	FP	1500	FP	FP	FP	FP	FP	FP	FP	FP	FP
69	299	12180	12250	1180	FN	FN	3180	3180	FP	FN	FP	FP	FN	FN	FN	FN	FP	430	FP	FP	FN	3180
70	293	13980	14500	FN	1980	1480	FN	FN	FN	FP	FP	FP	FN	FP	1980	FP	FP	1980	FN	FN	FP	FN
72	300	18600	28750	FP	FP	FP	FP	FP	FP	FP	FP	FP	FP	FP	FP	FP	FP	FP	FP	3600	FP	FP
74	214	17460	17750	FP	FP	2460	FP	FP	FP	FP	1960	FP	2210	FP	FP	FP	1710	FP	FP	FP	1210	1710
74	216	9840	20500	340	340	1590	590	FP	FP	340	1590	1090	1090	340	FP	1590	1590	FN	840	FP	2340	340
75	193	10680	11000	FP	930	930	930	2680	FP	FN	2430	FP	3180	FP	930	FN	FN	1930	FN	1430	1180	FP
81	199	22140	22500	FP	FP	FP	2640	2890	FP	FP	FP	FP	FP	FP	FP	FP	FP	FP	FP	FP	2890	FP
82	200	13620	16000	FP	FP	FP	FP	FP	870	FP	FP	FP	FN	FP	FP	FP	1120	FP	FN	FP	1870	FP
83	207	23760	29500	FP	FP	FP	3510	FN	FN	FP	3510	FP	FP	FP	FP	FP	FP	FP	FP	FN	FP	260
84	203	20220	20250	FP	FP	FP	FP	FP	FP	FP	FP	FP	FP	FP	FP	FP	FP	FP	FP	FP	FP	FP
86	211	18660	19000	FN	FN	FP	2910	FP	FP	FP	FP	FP	FN	FP	1160	FP	160	FP	FP	FP	FP	FN
89	222	9360	15250	FN	FP	FN	FN	3110	FN	FN	FN	FP	FN	FN	2610	2360	110	FP	FN	FP	FN	3110
90	221	11760	12750	FP	FN	FP	FP	FN	1510	FP	FN	FP	FN	FN	FP	FN	2760	FN	FN	FP	1760	FP
94	308	13080	13250	FP	FN	FP	80	FN	FP	FP	FP	FP	FN	FP	FP	FN	2080	FP	FP	FP	FP	FN
99	17	0	7000	TN	TN	TN	TN	TN	TN	TN	TN	TN	TN	TN	TN	TN	TN	TN	TN	TN	TN	TN
100	22	0	8250	TN	TN	TN	TN	TN	TN	TN	TN	TN	TN	TN	TN	TN	TN	TN	TN	TN	TN	TN

PID, patient identifier; DID, dataset identifier; FN, false negative; FP, false positive; TN, true negative; T(SZ), time of seizure (sec) from start of data; T(EN), time (sec) from the beginning to the end of the dataset, 0, no temporal lobe epilepsy event.

characterizations in Tables 1 and 2 were verified by double entry from the physician's final reports. Table 1 shows that patient age ranged from 4 to 57 years, including datasets from 36 female and 25 male patients. We examined all 19 EEG channels in each of these datasets, which have lengths between 5,000 seconds (1 hour 23 minutes) and 29,500 seconds (8 hours 12 minutes).

All scalp EEGs are obscured by muscular activity as a result of eye blinks, facial twitches, and so forth. These artifacts are avoidable by obtaining EEG data from depth or subdural electrodes, but such methods are invasive and nonambulatory. We remove most of the low-frequency artifacts from the scalp EEG data with a novel zero-phase quadratic filter, which—unlike standard linear filters—retains the nonlinear amplitude and phase relationships (Hively et al., 1995). This filter uses a moving window of $2n + 1$ points of raw EEG data, e_i, with the same number of data points, n, on either side of a central point. We fit the data to a quadratic equation, $F(t) = a_1T^2 + a_2T + a_3$, with $T = t - t_c$, and t_c the time at the central point of the moving window. We fit this quadratic form to the data, by minimizing $\Psi = \Sigma[F(t) - e_i]^2$, where the sum is over the $2n + 1$ points in the moving window. The minimum in Ψ is found from the condition $\delta\Psi/\delta a_k = 0$, which yields three linear equations in three unknowns. The window-averaged artifact at the central point is given by the fitted value at the central point $F(t_c = t_i) = a_3$. We note that the sums over odd powers of T_i are zero and that symmetric sums over even powers of T_i (over i from $-n$ to n) can be converted to sums from 1 to n, giving a window-averaged solution for the artifact signal

$$\begin{aligned} &F(t = t_c) \\ &\quad = [3(3n^2 + 3n - 1)(\Sigma e_{i+c}) - 15(\Sigma i^2 e_{i+c})]^2/ \\ &\quad (4n^2 + 4n - 3)(2n + 1). \end{aligned} \tag{16}$$

The sums in this last equation are over i from $-n$ to n, with sums over even powers of i evaluated explicitly with standard formulas. The effort to evaluate this equation can be reduced further by computing the sums initially from the previous equation with $c = n + 1$, and then using recursions thereafter (Hively et al., 1995). Application of this filter to the N-point set of raw EEG data, e_i, yields $N - 2n$ points of artifact data, f_i, that contain the low-frequency artifact signal. The residual (artifact-filtered) signal, $g_i = e_i - f_i$, has essentially no low-frequency artifact activity. The filter window width corresponds to eye blink activity at 2 Hz, for which $n = 62$ at a 250-Hz sampling rate. All subsequent EEG analysis uses this artifact-filtered data.

Fig. 5 compares the raw signal, conventional nonlinear measures, and PS dissimilarity measures for an epileptic event. Signal amplitude (Fig. 5a) shows little preevent variability except four small spikes between 450 and 750 seconds, followed by a large-amplitude spike during the event. Correlation dimension (Fig. 5b) shows two successive ($N_{occ} = 2$) threshold crossings ($U_{crit} = 3$) at 1,650 seconds, giving 282 seconds of forewarning without any subsequent indication of the event. The Kolmogorov entropy (Fig. 5c) varies erratically, with no forewarning or indication of the event. The first minimum in the MIF (Fig. 5d) has two successive threshold crossings at 1,760 seconds, giving 172 seconds of forewarning without any event indication.

The PS dissimilarity measures remain small for 1,200 seconds then all increase together above threshold at 1,320 seconds to provide 612 seconds of forewarning. These results illustrate the robustness and consistency of the PS dissimilarity measures for change indication, in sharp contrast to the lack of indication for the raw signal and inconsistent indication by the conventional nonlinear measures.

Fig. 6 compares the raw EEG signal, conventional nonlinear measures, and PS dissimilarity measures for a second epileptic EEG dataset. The raw EEG (Fig. 6a) shows a large spike at 7,190 seconds, with several small spikes before and after this large one. The event occurs at 11,280 seconds. The correlation dimension (Fig. 6b) shows quasiperiodic variability with no clear forewarning or event indication. The Kolmogorov entropy (Fig. 6c) also displays quasiperiodic variability before and after the event that provides no forewarning or indication of the event. The first minimum in the MIF (Fig. 6d) varies erratically with three successive values above threshold at 9,280 seconds (3,000 seconds of forewarning), then increases during the event to a value that is below the peak at 5,000 seconds. In sharp contrast to these inconsistent indications for the conventional measures, the PS dissimilarity measures all increase together with three successive values above threshold at 10,560 seconds, to provide 720 seconds of forewarning. Consequently, we focus the remainder of this analysis on the use of PS dissimilarity measures for condition change.

The choice of the base case is not obvious nor is it uncontroversial for EEG analysis. Consequently, we tested the robustness and consistency of the dissimilarity measures by offsetting the base case for a typical epileptic EEG dataset. Fig. 7a shows that the dissimilarity is low during the base case period (first 10 cut sets), subsequently increases, and then peaks during the event.

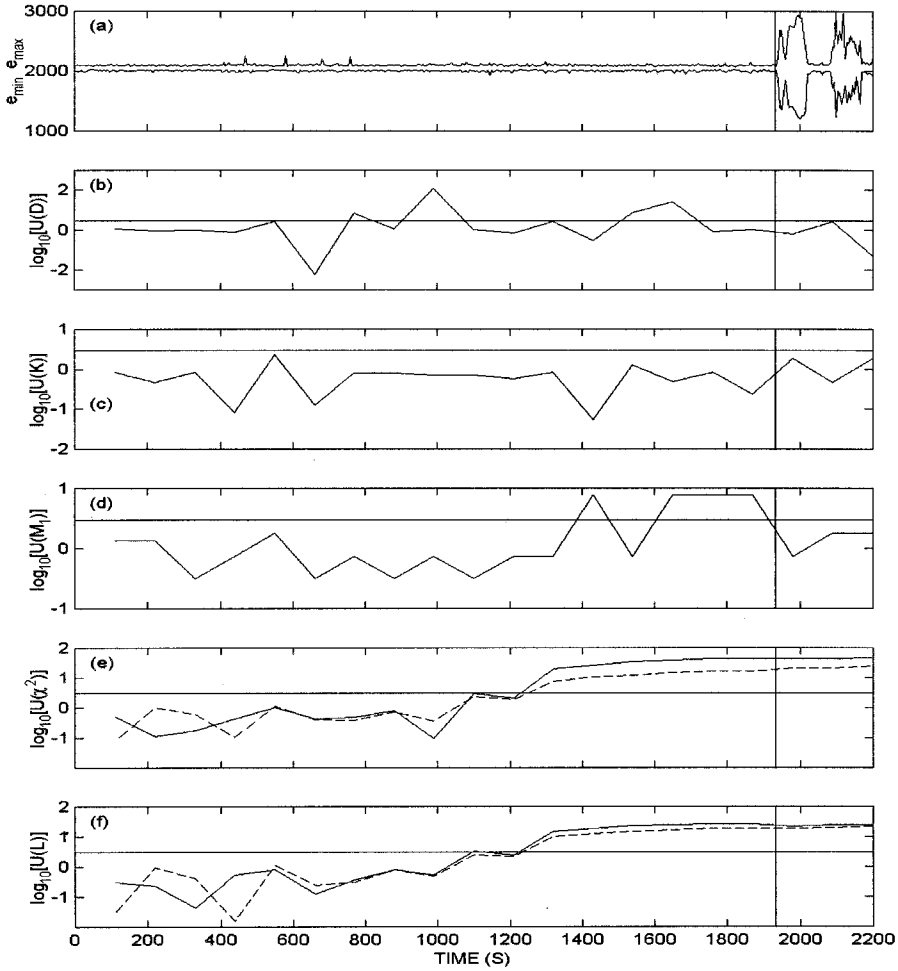

FIG. 5. Various measures versus time for channel T4 of dataset #SZPR03 (total dataset length of 2,215 seconds, sampled at 200 Hz) with seizure onset at 1,932 seconds (vertical line in each subplot): **(a)** smallest (e_{min}) and largest (e_{max}) values of the raw EEG signal in each cutset, **(b)** renormalized correlation dimension, **(c)** renormalized Kolmogorov entropy, **(d)** renormalized value of the first minimum in the mutual information function (M_1), **(e)** renormalized χ^2 measure for the non-connected- (solid) and connected-PS (–), and **(f)** renormalized L_1 measure for the non-connected (solid) and connected PS (–). We show a threshold of three (U_c=3) for this example in subplots e-f. The phase-space reconstruction parameters are: S=22, d=3, N=22,000. See text for discussion.

Fig. 7b shows that the dissimilarity is large initially, decreasing to low values during the base case period (cut sets 34 to 43), then subsequently increases to a peak during the event. Fig. 7c shows large values of dissimilarity at the beginning of the dataset that then decrease to small values during the base case (cut sets 66 to 75), then show a peak at the event. These results show that the dissimilarity is low during the base case and increases as the brain dynamics depart from the base case. We also note that the parameters for these results are different for the subsequent analysis (as found by a systematic search for the best parameters), thus illustrating the robustness of the method for less than "best" parameters.

Fig. 8 illustrates further the consistency of the dissimilarity measures for event forewarning. This patient had three successive epileptic events with separations of slightly more than 1 hour. The base case was taken at the beginning of the dataset (cut sets 1 to 10). All four dissimilarity measures detect each event, as well as provide more than 2,000 seconds of forewarning for each event. The PS reconstruction parameters are different from the earlier case (Fig. 5), as an additional demonstration of the method's robustness and consistency. To our knowledge, this example is the first demonstration of forewarning for multiple events in a single dataset by using nonlinear dynamics techniques. This result is not included with the 41 TL events in Table 2, because the event occurs only 45 minutes after the start of the data and is not detected as a true positive for the "best" parameter set. Nevertheless, the clear forewarning for each of the multiple events remains a success for the methodology.

We used an operational approach to find the best parameters for PS reconstruction and forewarning. In particular, we varied each parameter systematically with all the others fixed, to find the largest fraction of true positive plus true negative event forewarnings over the 61 datasets. We subsequently performed all analyses with the single best choice of the analysis parameters; namely, d = 3, N = 62 500, S = 16, N_{occ} = 16, and U_{crit} = 0.035. The values of x_{min},

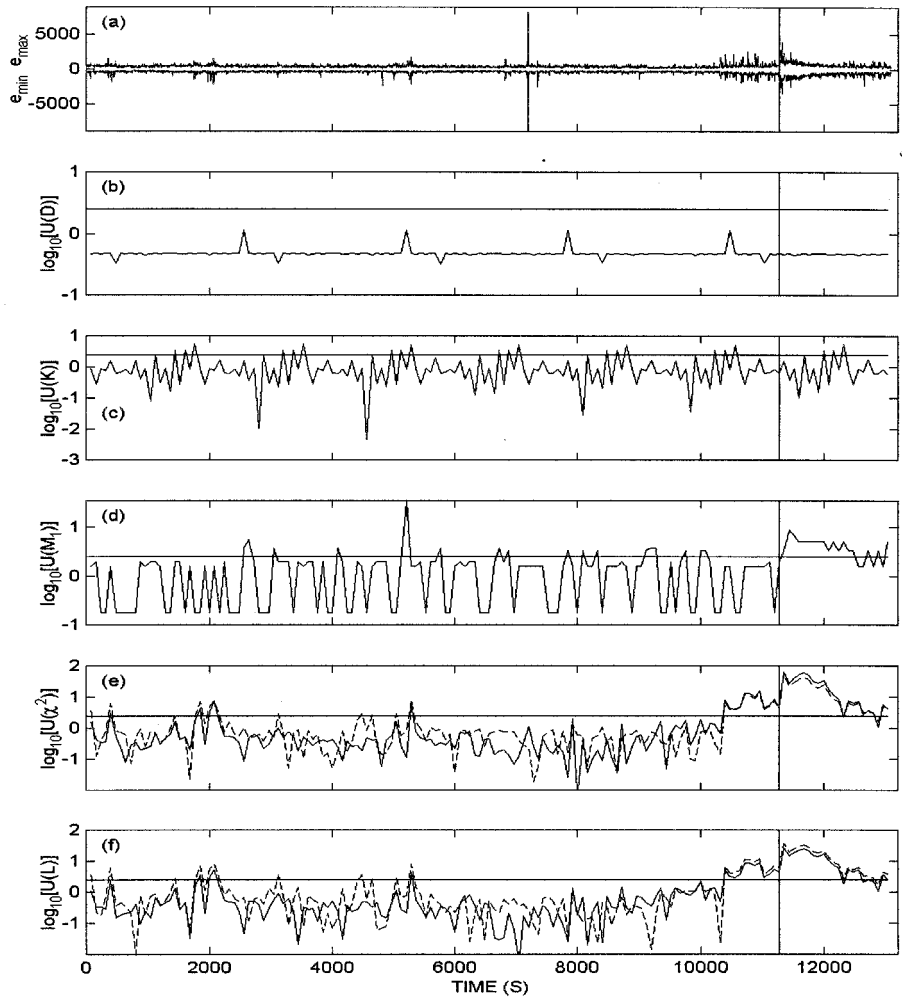

FIG. 6. Various measures versus time for channel F4 of dataset #20 with seizure onset at 11,280 seconds (vertical line in each subplot): **(a)** smallest (e_{min}) and largest (e_{max}) values of the raw EEG signal in each cutset, **(b)** renormalized correlation dimension, **(c)** renormalized Kolmogorov entropy, **(d)** renormalized value of the first minimum in the mutual information function (M_1), **(e)** renormalized χ^2 measure for the non-connected- (solid) and connected-PS (–), and **(f)** renormalized L_1 measure for the non-connected- (solid) and connected-PS (–). A typical threshold value (solid horizontal line in subplots e-f) is shown at U_c=2.5. The phase-space reconstruction parameters are: S=16, d=3, N=20,000. See text for discussion.

x_{max}, and M_1 are taken from the first cut set of each dataset. Systematic optimization over all the available parameters is the subject of future work.

Fig. 9 shows an example of no indication in a normal dataset. In particular, the four measures occur above the threshold, but do not remain there for the requisite number of successive occurrences to be counted as a positive indication. The choice of small U_{crit}. and large N_{occ} uses infrequent occurrences of small dissimilarity values to eliminate false negatives and false positives, as shown in Fig. 10. The topology of these contours remains surprisingly robust for a relatively large range of values of d, S, and N (not shown). Specifically, the total true rate (true positives plus true negatives) is small near the origin, and maximum inside an island at large N_{occ} and small U_{crit}. A subject of future work is systematic study of the total true rate versus N_{occ}, U_{crit}, d, S, and N.

Table 2 summarizes the forewarning times for all 61 datasets for the "best" choice of parameters. The total true rate is 59 of 61, including true positives for 39 of 41 TL events and true negatives for all 20 of the nonevent datasets. The PS dissimilarity method does not give true positives for two event datasets (nos. 203 and 286). For event datasets, we define a true positive as a forewarning time between 1 to 60 minutes in one or more channels, and a false positive as a forewarning time outside this range. This forewarning window represents the extreme limits for a "clinical useful" forewarning time for an epileptic event. Less than 1 minute is insufficient time for response to an impending event, and more than an hour is too nonspecific. The impact of other forewarning windows on the PS approach is the subject of future work. Our current analysis shows 70 to 3,600 seconds of forewarning for the 41 TL events, in up to 14 channels (dataset no. 216). For nonevent datasets, we define a true negative as no indication in one (or more) channels. Without a true negative indication in at least one channel of normal data, one is left with false indications in all channels, in which case the net indication

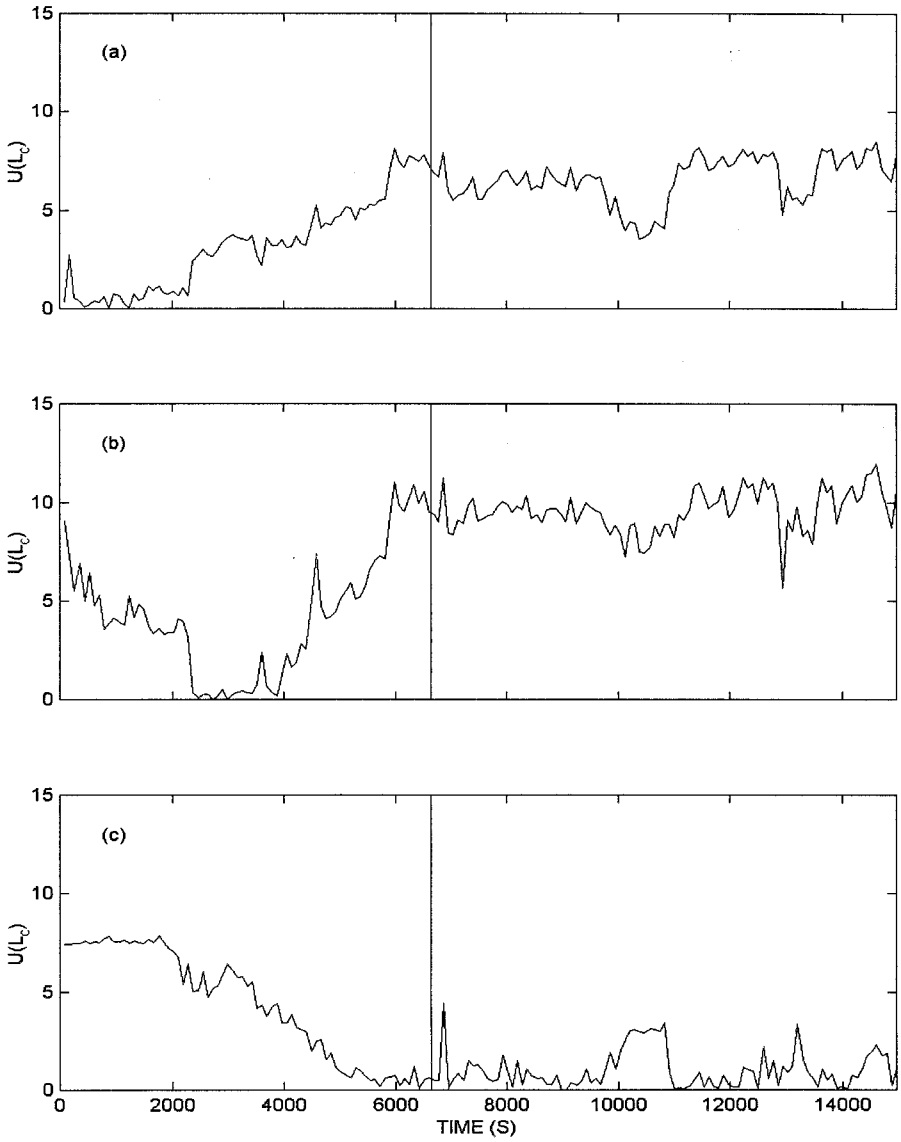

FIG. 7. Renormalized L_c dissimilarity measure versus time for channel F8 of dataset #PVM006 with seizure onset at 6,644 seconds (vertical line in each subplot): **(a)** basecase during the first ten cutsets, **(b)** basecase during cutsets 34-43, and **(c)** basecase during cutsets 66-75. The phase-space reconstruction parameters are: $S=22$, $d=3$, $N=22{,}000$. Other channels and the three other dissimilarity measures give similar results.

is a false positive. Based on the current analysis of model and EEG data, we conclude that the dissimilarity measures are superior to the conventional nonlinear measures as preevent indicators of condition change for a single channel of scalp EEG.

Detailed examination of Table 2 reveals three types of inconsistency. First, the "best" set of parameters provides forewarning for only the first event in each of the multiple-event datasets (dataset nos. 125, 222, 273, 287, and 386). Moreover, the "best" parameter set provides no forewarning for the any of the three events in dataset no. 129, as discussed earlier. Second, the forewarning channels for most TL events are inconsistent with the electrode with the earliest event indication (dataset nos. 170, 193, 199, 200, 203, 207, 211, 214, 221, 255, 264 to 267, 271, 286, 289, 299, 300, and 386). We do not regard this second inconsistency as serious, because the active electrode typically is oversensitive; in other words, it provides (false-positive) forewarning more than 1 hour before the event. Third, the channels with forewarning are inconsistent across multiple datasets from the same patient. We have denoted multiple datasets for each patient by bold-type identifiers in Table 2 to facilitate this discussion. For example, dataset no. 18 for patient no. 6 has forewarning in channels C4 and T4, whereas dataset no. 19 for patient no. 6 shows forewarnings in completely disjoint channels (O1, T6, FZ, and CZ). Channel FP1 shows inconsistent indication for patient no. 11 in three datasets out of four, with one true negative

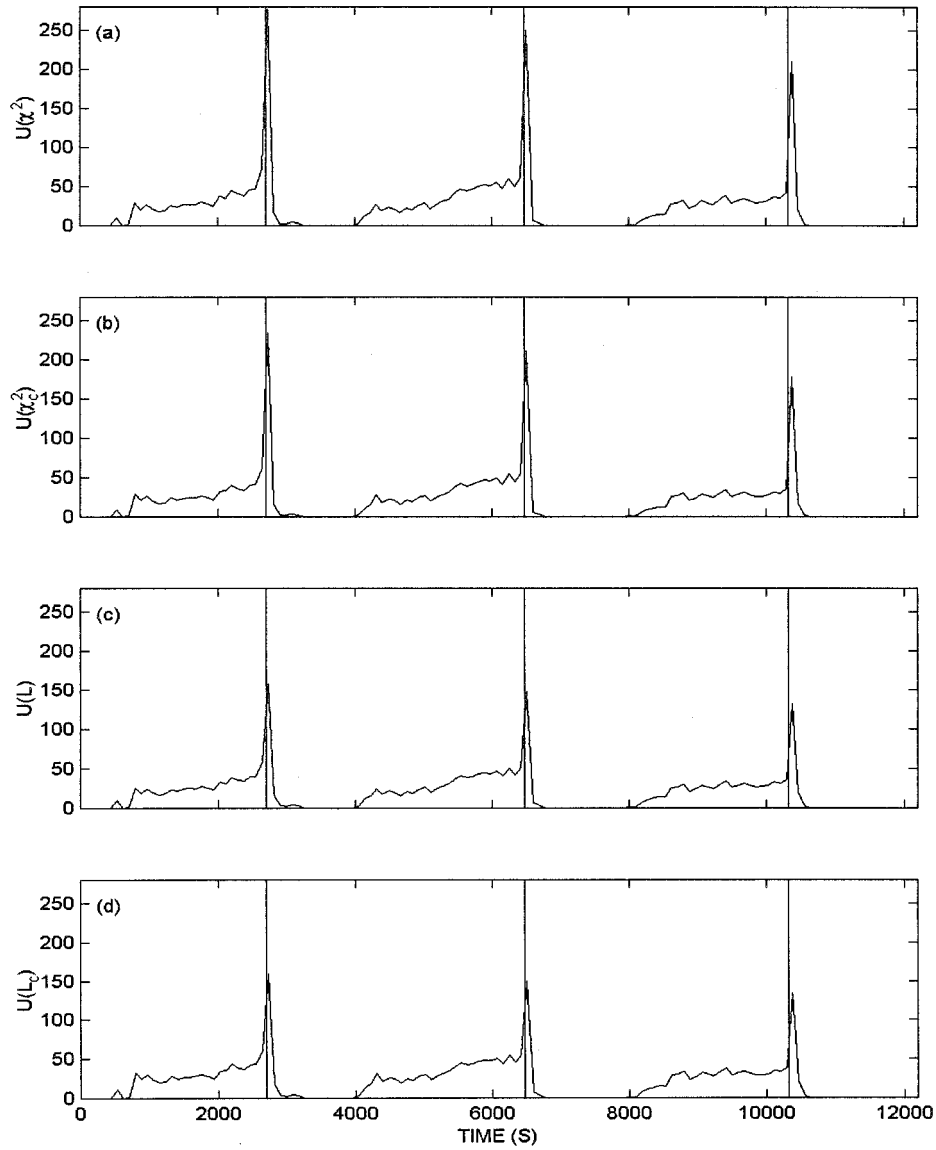

FIG. 8. Renormalized dissimilarity measures versus time for channel F3 of TLE dataset #129: **(a)** χ^2, **(b)** χ_c^2, **(c)** L, and **(d)** L_c, showing forewarning for three successive events with onset times at 2,700 seconds, 6,480 seconds, and 10,320 seconds (vertical lines in each subplot). The PS reconstruction parameters are: $S=22$, $d=3$, $N=22{,}000$. See text for discussion.

(dataset no. 37) and two forewarnings (dataset nos. 39 and 131). Channel FP2 gives inconsistent indications for patient no. 61 in three datasets (nos. 264, 266, and 271) out of five. Forewarning for patient no. 69 occurs in channel O2 for dataset no. 289 and in different channels (FP1, F4, C3, T5, and PZ) for dataset no. 299. This lack of uniformly true positives and negatives by channel violates assumption 10 and is the subject of future work, perhaps by finding the best PS reconstruction and forewarning parameters for multiple datasets from each patient.

DISCUSSION

One of the most important problems encountered in nonlinear time-series analysis is the appropriate characterization of changes in the system's dynamics. This problem is particularly vexing in physiologic systems, which are more often than not complex, nonstationary, affected by noise, and difficult to quantify fully in ordinary physical or mathematic terms. It is generally accepted that the brain behaves like a reasonably low-dimensional dynamic system with dynamics that may vary between (quasi-)periodic and completely irregular (chaotic). Thus, to a certain extent, global aspects of brain dynamics may be quantified legitimately by traditional nonlinear descriptors such as Lyapunov exponents, Kolmogorov entropy, and correlation dimension. Although these descriptors are adequate for discriminating between clear-cut regular and chaotic dynamics, they are

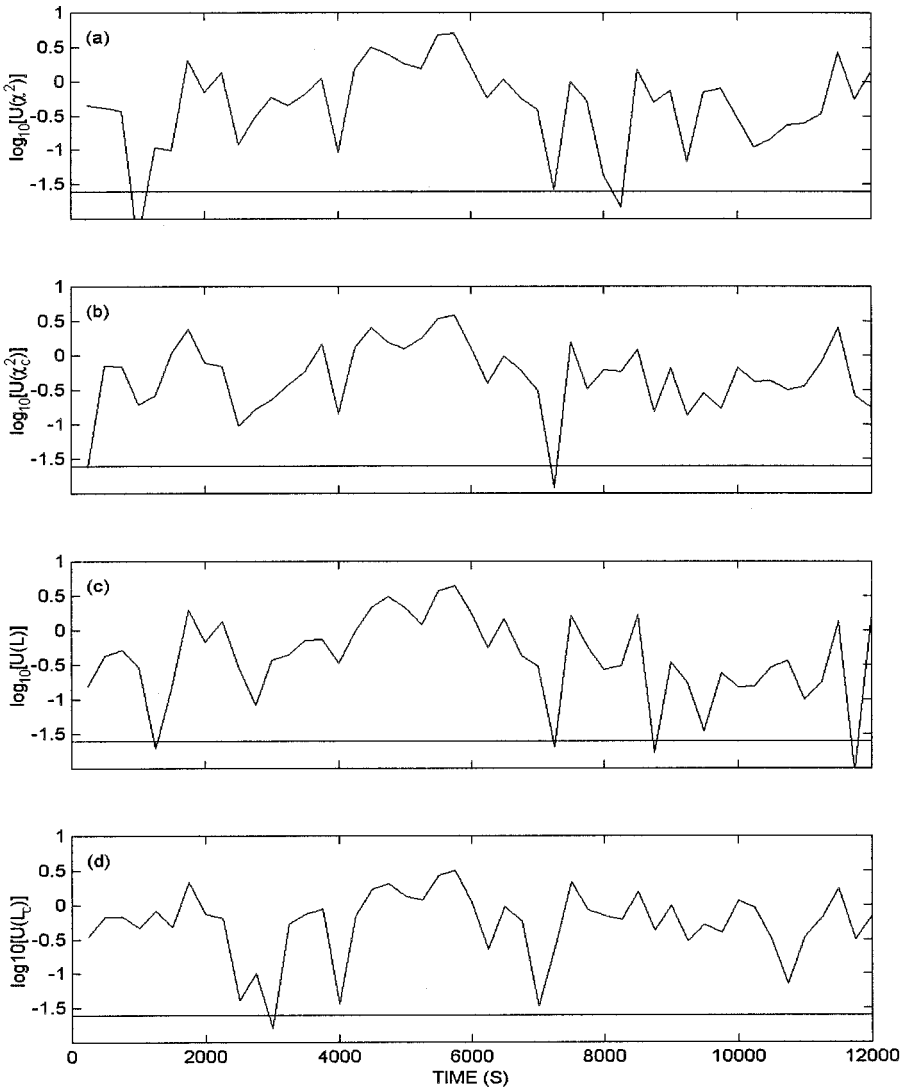

FIG. 9. Renormalized nonlinear measures versus time for channel FP2 of non-event dataset #165: **(a)** non-connected χ^2 measure, **(b)** connected-χ^2 measure, (c) non-connected L_1 measure, and **(d)** connected-L_1 measure. The threshold (horizontal line in each subplot) is set at the "best" value of U_c=0.025. The phase-space reconstruction parameters are: S=16, d=3, N=62,500. See text for discussion.

not sufficiently sensitive to distinguish quasiperiodicity, intermittency, or slightly different chaotic regimes, especially when data are limited and/or noisy. Unfortunately, most brain dynamics before, during, and after an epileptic event fall within the latter regime. Therefore, robust and timely forewarning of epileptic events has remained an outstanding challenge. We address this problem, by introducing four new measures of dissimilarity that capture more details about the dynamics and differences between various regimes and therefore are more sensitive than the traditional nonlinear measures. A change in these measures signifies that the system has departed from the base case and can be interpreted as a forewarning of an impending epileptic event.

The PS indicators of condition change measure the difference between PS density functions for a base case and a test case as χ^2 statistic and L_1 distance. Thus, these indicators retain the differences between the process dynamics and avoid the inner cancellation effects resulting from averaging over many orbits (as one does, for instance, when calculating the correlation dimension and the Kolmogorov entropy). Changes in the Lorenz and Bondarenko model dynamics are clearly detected by the dissimilarity measures and somewhat by the Kolmogorov entropy, as c increases from 5 to 18 (Figs. 1 and 4). On the other hand, these changes are either undetected or barely detected by the correlation dimension and mutual information measures. The new measures also indicate marked preevent changes in 39 of 41 TL datasets and 20 of 20 nonevent datasets (Table 2). These results show that the PS measures seem superior to traditional nonlinear measures for detection of condition change.

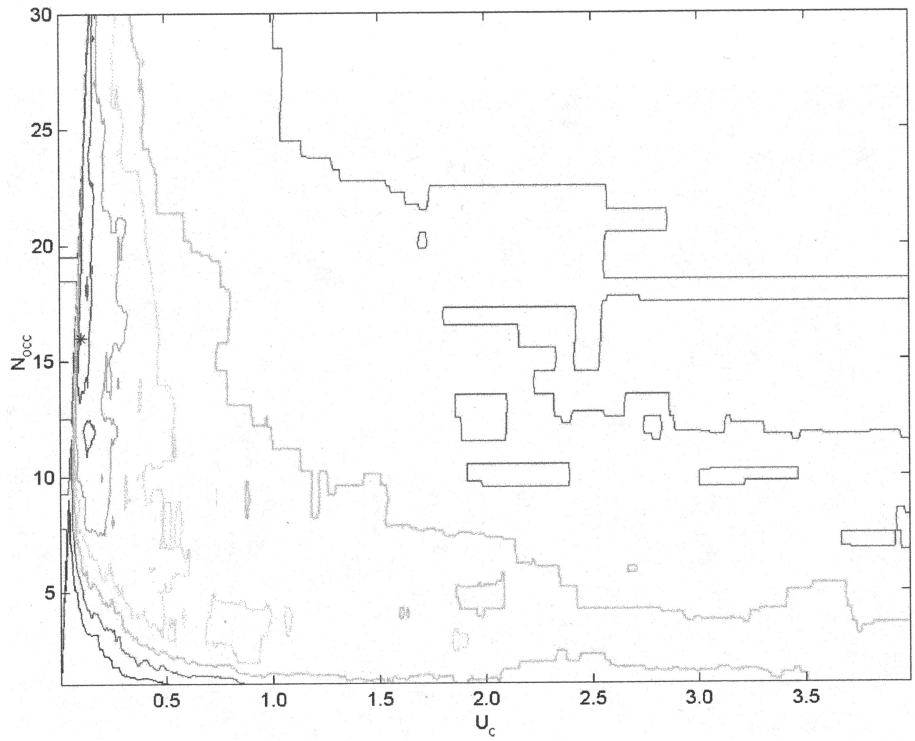

FIG. 10. Contours of constant total true rate versus U_c and N_{occ} for the best set of PS-reconstruction parameters of $d=3$, $S=16$, $N=62{,}500$. The contour levels begin at 0.1 and increase in steps of 0.1 to a maximum of 0.9. The largest total true rate (0.97) is located at $U_c=0.035$ and $N_{occ}=16$, as indicated by the asterick (*). See text for discussion.

Our approach differs from earlier work in the following respects. First, previous studies (Iasemidis and Sackellares, 1996; Lehnertz and Elger, 1998; Le van Quyen et al., 1999; Martinerie et al., 1998) used multichannel data from subdural and depth electrodes to avoid low-frequency (e.g., eye blink) artifacts. Instead, we analyze 19 channels of scalp EEG data that may eventually allow for noninvasive, ambulatory, long-term, nonclinical monitoring. Second, we remove the low-frequency artifacts from scalp EEG with a novel zero-phase quadratic filter. Third, prior investigations forewarn via changes in conventional nonlinear measures, such as correlation integral (Casdagli et al., 1996; Le van Quyen et al., 1999; Martinerie et al., 1998), correlation dimension (Lehnertz and Elger, 1998), and largest Lyapunov exponent (Iasemidis and Sackellares, 1991, 1996; Le van Quyen et al., 2001). In our earlier work, we determined no consistent trends in such conventional nonlinear measures for various event types (Hively et al., 1995, 1999, and 2000a and 2000b). Therefore, we focused on PS dissimilarity measures without regard to event type. Fourth, our studies demonstrate methodology robustness over a variety of clinical conditions: digital and analog EEG from several clinical sites; data sampling at 200, 250, and 512 Hz; raw EEG data precision between 10 to 12 bits; presence of substantial noise in the raw EEG, as well as periods of constant signal; use of a fixed channel (namely, channel 13) in the bipolar montage; and use of a variety of clinically interesting channels in the 10/20 montage.

It is important to note that the PS indicators contain more information than we have systematically exploited so far. For instance, some datasets show a remarkably close similarity between the pairs $\{\chi^2, L\}$ and $\{L_c, \chi_c^2\}$, whereas other datasets show close similarities between $\{L, L_c\}$ and $\{\chi^2, \chi_c^2\}$. Other datasets show no similarities at all. The first situation may arise because the base case and test case DFs are not notably different from zero on a common domain. The second situation can be interpreted as a sign of very slow dynamics (little change between the PS and CPS measures). The third case displays more variability in the dynamics.

Despite the aforementioned progress, we assess our success to date as modest. As mentioned earlier, our analysis of epileptic events is *not a clinical analysis*, but rather an illustration of our method and its potential for event forewarning. Event forewarning is a formidable task, and the possibilities to fall into various traps are countless, as illustrated by various counterexamples that we have constructed to many situations that seem otherwise natural. Moreover, the EEGs for our analysis were obtained in a controlled clinical setting, which is very different from the uncontrolled environment where a portable, ambulatory device may attempt forewarning. In

addition, assumption 7 defines a forewarning as a true-positive indication in at least one channel, which is a rather weak criterion. Finally, we have adjusted the PS reconstruction and forewarning parameters that give the best rate of true positives plus true negatives for these 61 datasets. The algorithm may not be equally well tuned for other datasets. Thus, we are acutely aware that as long as the dynamics are *unknown*, they *may* reserve *any* surprise.

On the other hand, the performance and robustness of our approach on model data and real EEG suggests that this methodology could allow convenient electrode placement by a patient in a nonclinical, ambulatory setting and could be used as a complementary quantitative method in conjunction with clinical assessment. Future use of this approach as a complementary and/or stand-alone method for seizure forewarning will require extensive analysis of several events for each patient, and detailed determination of detection criteria. Future work will involve statistical evaluation of false positives and negatives in epileptic patients, and of false positives in normal patients; clinical monitoring of each patient to determine optimal PS reconstruction parameters, which subsequently would be fixed for ambulatory monitoring; the specific nonlinear features for event forewarning in the EEG; and the response of our approach to psychiatric states, such as hysterical events.

Acknowledgments: The authors thank Nicolet Biomedical Inc. (Madison, WI, USA) for supplying and characterizing the digital EEG data from five clinical sites. They also thank Dr. Raj Sheth (Department of Neurology, University of Wisconsin Medical School) for his clinical input to this research.

REFERENCES

Abarbanel HDI, Brown R, Sidorowich JJ, Tsimring LS. The analysis of observed chaotic data in physical systems. *Rev Mod Phys* 1993; 65:1331–92.

Abarbanel HDI, Kennel MB. Local false nearest neighbors and dynamical dimensions from observed chaotic data. *Phys Rev E* 1993;47: 3057–68.

Abarbanel HDI. *Analysis of observed chaotic data*. New York: Springer, 1996.

Abramovitz M, Stegun IA. *Handbook of mathematical functions*. New York: , 1964.

Babloyantz A, Destexhe A. Low dimensional chaos in an instance of epilepsy. *Proc Natl Acad Sci U S A* 1986;83:3513–7.

Bondarenko VE. Analog neural network model produces chaos similar to the human EEG. *Int J Bifurc Chaos* 1997;7:1133–40.

Cao L. Practical method for determining the minimum embedding dimension for a scalar time series. *Physica D* 1997;110:43–59.

Casdagli MC, Iasemidis LD, Sackellares JC, Roper SN, Gilmore RL, Savit RS. Characterizing nonlinearity in invasive EEG recordings from temporal lobe epilepsy. *Physica D* 1996;99:381–99.

Cover A, Reneke J, Lenhart S, Protopopescu V. RKH space methods for low level monitoring and control of nonlinear systems. II. A vector case example: the Lorenz system. *Math Models Methods Appl Sci* 1997;7:823–45.

Diks C, van Zwet W, Takens F, DeGoede J. Detecting differences between delay vector distributions. *Phys Rev E* 1996;53:2169–76.

Eckmann JP, Ruelle D. Ergotic theory of chaos and strange attractors. *Rev Mod Phys* 1985;57:617–55.

Elbert T, Ray WJ, Kowalik ZJ, Skinner JE, Graf EE, Birbaumer N. Chaos and physiology: deterministic chaos in excitable cell assemblies. *Physiol Rev* 1994;74:1–47.

Frank GW, Lookman T, Nerenberg MAH, Essex C, Lemieux J, Blume W. Chaotic time series analyses of epileptic events. *Physica D* 1990;46:427–38.

Fraser AM, Swinney HL. Independent coordinates for strange attractors from mutual information. *Phys Rev A* 1986;33:1134–40.

Gailey PC, Hively LM, Protopopescu VA. Robust detection of dynamical change in scalp EEG. In: *Proceedings of the 5th experimental chaos conference, June 28-July 1, 1999, Orlando, Florida (ECC5)*.

Grebogi C, Ott E, Yorke JA. Unstable periodic orbits and the dimensions of multifractal chaotic attractors. *Phys Rev A* 1988;37:1711–24.

Gribkov V, Gribkova D. Learning dynamics from nonstationary time series: analysis of electroencephalograms. *Phys Rev E* 2000;61: 6538–45.

Hively LM, Clapp NE, Daw CS, Lawkins WF. *Nonlinear analysis of EEG for epileptic events*. ORNL/TM-12961. Oak Ridge, TN: Oak Ridge National Laboratory, 1995.

Hively LM, Gailey PC, Protopopescu VA. Detecting dynamical change in nonlinear series time series. *Phys Lett A* 1999;258:103–14.

Hively LM, Gailey PC, Protopopescu VA. In: Lehnertz K, et al., eds. *Proceedings of the International Workshop. ''Chaos in Brain?,'' Bonn, Germany, 10–12 March:1999*. Singapore: World Scientific, 2000*a*:333–6.

Hively LM, Protopopescu VA, Gailey PC. Timely detection of dynamical change in scalp EEG signals. *Chaos* 2000*b*;10:864–75.

Iasemidis LD, Sackellares JC. The evolution with time of the spatial distribution of the largest Lyapunov exponent on the human epileptic cortex. In: Duke D, Pritchard W, eds. *Measuring chaos in the human brain*. Singapore: World Scientific, 1991:49–82.

Iasemidis LD, Sackellares JC. Chaos theory and epilepsy. *Neuroscientist* 1996;2:118–26.

Ivanov DK, Posch HA, Stumpf C. Statistical measures derived from the correlation integrals in physiological time series. *Chaos* 1996;6: 243–53.

Jackson EA. *Perspectives of nonlinear dynamics*. Vol. 1. Cambridge: Cambridge University Press, 1989.

Jackson EA. *Perspectives of nonlinear dynamics*. Vol. 2. Cambridge: Cambridge University Press, 1990.

Jeong J, Kim MS, Kim SY. Test for low-dimensional determinism in electroencephalograms. *Phys Rev E* 1999;60:831–7.

Kantz H, Schreiber T. *Nonlinear time series analysis*. Cambridge: Cambridge University Press, 1997.

Lehnertz K, Elger CE. Can epileptic events be predicted? Evidence from nonlinear time series analysis of brain electrical activity. *Phys Rev Lett* 1998;80:5019–22.

Lerner DE. Monitoring changing dynamics with correlation integrals: case study of an epileptic event. *Physica D* 1996;97:563–76.

Letellier C, Maquet J, Le Sceller L, Gouesbet G, Aguirre LA. On the non-equivalence of observables in phase-space reconstructions from recorded time series. *J Phys A* 1998;31:7913–27.

Le Van Quyen M, Martinerie J, Baulac M, Varela F. Anticipating epileptic events in real time by a nonlinear analysis of similarity between EEG recordings. *Neuroreport* 1999;10:2149–55.

Le Van Quyen M, Martinerie, Navarro V, et al. Anticipation of epileptic events from standard EEG recordings. *Lancet* 2001;357:183–8.

Lorenz EN. Deterministic nonperiodic flow. *J Atmos Sci* 1963;20:130–41.

Manuca R, Savit RS. Stationarity and nonstationarity in time series analysis. *Physica D* 1996;99:134–61.

Manuca R, Casdagli MC, Savit RS. Nonstationarity in epileptic EEG and implications for neural dynamics. *Math Biosci* 1998;147:1–22.

Martinerie J, Adam C, Le Van Quyen M, et al. Epileptic events can be anticipated by nonlinear analysis. *Nat Med* 1998;4:1173–6.

Moeckel BR, Murray B. Measuring the distance between time series. *Physica D* 1997;102:187–94.

Mood AM, Graybill SA, Boes DC. *Introduction to the theory of statistics*. New York: McGraw Hill, 1974.

Osorio I, Frei MG, Wilkinson SB. Real-time automated detection and quantitative analysis of events and short term prediction of clinical onset. *Epilepsia* 1998;39:615–27.

Pezard L, Martinerie J, Breton F, Bourzeix JC, Renault B. Nonlinear forecasting measurements of multichannel EEG dynamics. Electroencephalogr *Clin Neurophysiol* 1994;91:383–91.

Pezard L, Martinerie J, Mueller–Gerking J, Varela FJ, Renault B. Entropy quantification of human brain spatio-temporal dynamics. *Physica D* 1996;96:344–54.

Pradhan N, Sadasivan PK. Validity of dimensional complexity measures of EEG signals. *Int J Bifurc Chaos* 1997;7:173–86.

Protopopescu V, Hively LM, Gailey PC. Robust forewarning of dynamical change from single channel scalp EEG data. In: AQ *Proceedings of the 18th Energy Symposium on Energy Sciences.* May 15–16, 2000. AQ:137–45.

Qu H, Gotman J. A patient specific algorithm for the detection of event onset in long-term EEG monitoring: possible use as a warning device. IEEE *Trans Biomedical Eng* AQ1997;44:11522.

Quian Quiroga R, Arnhold J, Lehnertz K, Grassberger P. Kuhlback–Leibler, renormalized entropies. Applications to electroencephalograms of epilepsy patients. *Phys Rev E* 2000;62:8380–6.

Rezek A, Roberts SJ. Stochastic complexity measures for physiological signal analysis. IEEE *Trans Biomed Eng* 1998;45:1186–91.

Sauer T, Yorke J, Casdagli M. Embedology. *J Stat Phys* 1991;65:579–616.

Schiff SJ, Jerger K, Duong DH, Chang T, Spano ML, Ditto WL. Controlling chaos in the brain. *Nature (Lond)* 1994;370:615–20.

Schouten JC, Takens F, van den Bleek CM. Maximum likelihood estimation of the entropy of an attractor. *Phys Rev E* 1994a;49:126–9.

Schouten JC, Takens F, van den Bleek CM. Estimation of the dimension of a noisy attractor. *Phys Rev E* 1994b;50:1851–61.

Schreiber AT. Detecting and analyzing nonstationarity in a time series using nonlinear cross predictions. *Phys Rev Lett* 1997;78:843–6.

Schreiber T. Interdisciplinary application of nonlinear time series methods. *Phys Rep* 1999;308:1–64.

Shannon CE, Weaver W. *The mathematical theory of communication*. Urbana: University of Illinois Press, 1949.

Takens F. *Dynamical systems, turbulence*. New York: Springer, 1981: 366, [Lecture notes in mathematics vol. 898.]

Takens F. On the numerical determination of the dimension of an attractor. In: *Lecture notes in mathematics*. Vol. 1125. Berlin: Springer, 1984:99–106.

Thomasson N, Hoeppner TJ, Webber CL Jr, Zbilut JP. Recurrence quantification in epileptic EEGs. *Phys Lett A* 2001;279:94–101.